PASJ: Publ. Astron. Soc. Japan , 1–??,

An SiO Maser Search off the Galactic Plane

Shuji Deguchi,[1] Takahiro Fujii,[2,3] Yoshifusa Ita,[4,5], Hiroshi Imai,[2,3],
Hideyuki Izumiura,[6] Osamu Kameya,[7] Noriyuki Matsunaga,[4] Atsushi Miyazaki,[1,7,8]
Arihiro Mizutani,[9,10] Yoshikazu Nakada,[4] Jun-ichi Nakashima,[1,11]
and
Anders Winnberg[1,12]

[1] *Nobeyama Radio Observatory, National Astronomical Observatory, Minamimaki, Minamisaku, Nagano 384-1305*
[2] *VERA Project Office, National Astronomical Observatory, 2-21-1 Osawa, Mitaka, Tokyo 181-8588*
[3] *Faculty of Science, Kagoshima University, 1-21-35 Korimoto, Kagoshima 890-0065*
[4] *Institute of Astronomy, School of Science, The University of Tokyo, 2-21-1 Osawa, Mitaka, Tokyo 181-0015*
[5] *Institute of Space and Astronautical Science, Japan Aerospace Exploration Agency, Yoshinodai 3-1-1, Sagamihara, Kanagawa 229-8510*
[6] *Okayama Astrophysical Observatory, National Astronomical Observatory, Kamogata, Asakuchi, Okayama 719-0232*
[7] *Mizusawa VERA Observatory, National Astronomical Observatory, Mizusawa, Oshu, Iwate 023-0861*
[8] *Shanghai Astronomical Observatory, Chinese Academy of Sciences 80 Nandan Road, Shanghai, 200030, P.R. China*
[9] *Department of Astronomical Science, The Graduate University for Advanced Studies, 2-21-1 Osawa, Mitaka, Tokyo 181-8588*
[10] *Koriyama City Fureai Science Center, 2-11-1 Ekimae, Koriyama, Fukushima 963-8002*
[11] *Academia Sinica, Institute of Astronomy and Astrophysics, P.O. Box 23-141, Taipei 106, Taiwan*
[12] *Onsala Space Observatory, 439 92 Onsala, Sweden*

(Received 2006 December 18; accepted 2007 March 27)

Abstract

We have searched for the SiO $J = 1$–0 $v = 1$ and 2 maser lines at ~ 43 GHz in 277 2MASS/MSX/IRAS sources off the Galactic plane ($|b| \gtrsim 3^\circ$), which resulted in 119 (112 new) detections. Among the new detections, are two very faint objects with MSX 12μm flux densities below 2 Jy. These are likely to be O-rich AGB-stars associated with dwarf-galaxy tidal tails. The sample also includes medium bright MSX objects at moderately high Galactic latitudes ($3^\circ < |b| < 5^\circ$) and in the IRAS gap at higher latitudes. A signature of a warp of the inner Galactic disk is found for a disk subsample. This warp appears relatively strongly in the area of $0 < l < 45^\circ$ and $3 < |b| < 5^\circ$. We also found a group of stars that does not follow to the Galactic rotation. This feature appears in the Galactic disk at $l \sim 27^\circ$, and extends more than 15° in Galactic latitude, like a stream of tidal debris from a dwarf galaxy.

Key words: Galaxy: halo, kinematics and dynamics — masers — stars: AGB and post-AGB

1. Introduction

Stellar maser sources are good tracers of Galactic structure. They are mostly AGB (Asymptotic Giant Branch) stars with typical ages of a few Gyr, representing a dynamically well-relaxed component of the Galaxy. Large surveys of maser sources have been made using the OH 1612 MHz line in the past towards objects in the Galactic plane within $|l| < 45^\circ$ and $|b| < 3^\circ$ (Sevenster et al. 1997; Sevenster et al. 2001), or using the 43 GHz ($J = 1$–0 $v = 1$ and 2) SiO maser lines toward the Galactic bulge (Izumiura et al. 1995), inner and outer disk (Deguchi et al. 2004b; Jiang et al. 1996), and the Galactic center (Deguchi et al. 2004a; Fujii et al. 2006), or with the 86 GHz ($J = 2$–1 $v = 1$) SiO maser line in a thinner strip $|b| \lesssim 1^\circ$ (Messineo et al. 2002). However, because of a relative scarcity of sources off the Galactic plane ($|b| > 3^\circ$), all-sky surveys for the maser sources were not made much in the past (except for te Lintel-Hekkert et al. 1991 or Ita et al. 2001). Because of recent studies of halo substructure (Ibata et al. 2001a) and it's dynamical influence on the disk structure of the Galaxy (Binney 2001), it is worth looking among SiO maser survey data for signatures of dwarf galaxies in the Galactic halo. In fact, the MSX survey, which was a large deep survey of infrared objects after IRAS, contained data from the Galactic disk

($|b|<6^\circ$) and additional higher-latitude objects in the limited area that IRAS could not access (the "IRAS gap"). Many of these higher-latitude objects were not searched for masers in the past simply because they were absent from the IRAS Point Source Catalog, even though they are bright in the infrared.

In this paper, we report on the results of SiO maser searches for objects outside the Galactic plane. The sample contains very bright to unusually faint IR sources, because they originate from several observation programs with different rationales. Some of them are very distant objects for which SiO masers were never thought to be detectable, and therefore interesting in themselves.

2. Observations

Simultaneous observations in the SiO $J=1$–0, $v=1$ and 2 transitions at 42.122 and 42.821 GHz respectively were made with the 45m radio telescope at Nobeyama mainly during the winter–spring seasons between 2003 –2006: in addition a few unpublished results from 1999 and 2000 were included in this work. We used a cooled SIS mixer receiver (S40) for the 43 GHz observations and accousto-optical spectrometer arrays, AOS-H and AOS-W, having bandwidths of 40 and 250 MHz respectively. The effective velocity resolution of the AOS-H spectrometer was 0.3 km s^{-1}. The arrays covered the velocity range of $\pm$380 km s^{-1} (except for the 2006 observations which had a $\pm$150 km s^{-1} coverage), for both the SiO $J=1$–0 $v=1$ and 2 transitions simultaneously. The overall system temperature was between 200 and 300 K, depending on weather conditions. The half-power telescope beam width (HPBW) was about 40″. The antenna temperature is corrected for atmospheric and telescope ohmic loss, but not for the beam or aperture efficiency ($T_{\rm a}^*$). The factor for conversion between antenna temperature and flux density is about 2.9 Jy K^{-1}. Further details of SiO maser observations using the NRO 45-m telescope have been described elsewhere (Deguchi et al. 2000a).

The objects in the present work originate from several different observing programs, which were partially backup programs during times when the weather was unsuitable for higher frequency observations. Therefore, results from several different categories of objects are presented here. A majority of our objects are MSX sources off the Galactic plane in the area, $0^\circ<l<45^\circ$ and $3^\circ<|b|<6^\circ$; these objects are mostly excluded from our previous systematic SiO surveys of the Galactic plane, which were limited to the strip with $|b|<3^\circ$ (Deguchi et al. 2004b). A second group of objects are MIR sources from the $|b|>6^\circ$ MSX catalog (Egan et al. 2003) in the IRAS gap; these are often bright MIR objects with no IRAS record and as a result they have not been thoroughly investigated before. The third group of objects are very faint stars which were chosen for the search for AGB stars from halo dwarf galaxies. These objects are mostly located at high Galactic latitudes; they exhibit star-like red images on 2MASS JHK-band images, but the AGB nature of these objects has not been well established due to their faintness in the infrared bands. These objects were selected by customary color-index criteria for SiO maser searches (Deguchi et al. 2004b): $H-K>0.5$, and $-0.5\lesssim C_{CE}\lesssim 0.5$. Here $C_{CE}=log(F_E/F_C)$, and F_C and F_E are the MSX flux densities in the C(12 μm) and E(21 μm) bands. The K magnitude and the 12 μm flux density are measures of distance to the source. On average, the mass losing AGB stars at about 8 kpc (as for stars in the Galactic bulge) typically have a color-corrected K magnitude of $\sim$6 and a 12 μm flux density of $\sim$4 Jy (for objects with an effective dust-shell temperature of 300 K). Therefore, when searching distant objects, like those of Sgr Dwarf galaxy and it's tail ($D\sim$ 16–24 kpc), we have to look for faint objects with $K\gtrsim 8$ and $F_C\sim 1$ Jy or less. For the case of CMa dwarf ($D\sim$ 7 kpc), the flux limitation is slightly relaxed. In order to search for SiO masers in such a distant object, we have to observe all the brighter objects in the same area to get a good idea of the velocity field of foreground Galactic sources. Thus, we included the brighter objects in front of the dwarf galaxies in the survey, especially for the bulge sources toward Sgr dwarf galaxy (center at $l=5^\circ$ and $b=-14^\circ$; Majewski et al. 2003). For the case of the CMa dwarf (center at $l=240^\circ$ and $b=-8^\circ$; Martin et al. 2004a), it is problematic too because the distance is around 7 kpc and some of objects spread toward the Galactic disk. For the survey, we chose faint red objects within 30 degree of the center of the CMa dwarf.

We searched for the SiO $J=1$–0 $v=1$ and 2 maser lines in 277 objects and detected 119 (112 new) sources. The detected sources are summarized in table 1 and the undetected sources in table 2. The distribution of the observed sources on the sky is shown in figure 1. Table 3 lists the IR properties of the observed sources: 2MASS name, 2MASS K magnitude, $J-H$ and $H-K$ color indices, MSX 6C name, position differences between 2MASS and MSX sources, MSX C-band (12μm) flux densities, $C_{AC}=log(F_C/F_A)$ and $C_{CE}=log(F_E/F_C)$, and IRAS name and its' separation from the 2MASS position. The 2MASS K magnitude and MSX C-band (12 μm) flux density are plotted against color index of the observed objects in the left and right panels of figure 2, respectively. Though the observed objects involved a wide range of flux densities in terms of 2MASS K or MSX C band compared with those of other well defined survey programs, the color indices of the objects were limited to a reasonable range for SiO detections (Deguchi et al. 2000a; Deguchi et al. 2004b; Fujii et al. 2006). Our sample involves 25 AGB candidates for dwarf galaxy associations, which resulted in 3 SiO detections. We discuss individual objects separately in Appendix A and provide the 112 spectra of our new detections there.

3. Discussion

The observed radial velocities are plotted against Galactic longitude in figure 3. Velocities expected from Galactic rotation are shown by solid and broken curves for various galactocentric distances. The data have been divided into two sub-samples: one 'disk sample' with

$|b| < 10^\circ$ and one 'high-latitude sample' with $|b| > 10^\circ$. There is a hint in the upper panel of figure 3 that the disk sample (open circles) follows the Galactic rotation curve better than the high-latitude sample (filled triangles). Most of the high-latitude objects are supposedly Galactic bulge stars, so deviations of up to about 100 km s^{-1} from the Galactic rotation are to be expected (Izumiura et al. 1995).

3.1. AGB candidates for dwarf galaxy associations

The Sgr dwarf elliptical galaxy (SagDEG) was discovered by Ibata et al. (1994) at $V_{hel} = 140$ km s^{-1} toward the Galactic bulge. Its distance was estimated to be approximately 24 kpc from the Sun. Later investigations have confirmed the associations of M54 and other globular clusters with this dwarf galaxy, and moreover its associated trail of stars along its orbit being almost perpendicular to the Galactic plane (Ibata et al. 2001b). The trail includes a number of C-rich AGB stars (Ibata et al. 2001a) and M giants (Majewski et al. 2003). Therefore, the idea of looking for O-rich mass-losing AGB stars is not far-fetched, though the low-metal low-mass stars tend to become carbon-rich stars at the AGB phase of stellar evolution (Iben 1981; Ibata et al. 2001b). In fact, an SiO maser source have been detected in the Large Magellanic cloud with the SEST 15m telescope at 86.2 GHz (van Loon et al. 1996; see also Wood et al. 1992 for OH/IR sources).

An enhanced stellar density was found toward the anticenter region in the Sloan Digital Sky Survey (Yanny et al. 2003), suggesting that this is also a remnant of adwarf galaxy. The center of this enhanced density was estimated to be $l = 240$–244°, $b = -8$ – -10°, and this was named as CMa dwarf galaxy (Bellazzini et al. 2004; Martin et al. 2004b). Because the distance and radial velocity of the CMa dwarf galaxy are estimated to be 7.2 ± 0.3 kpc and 109 ± 4 km s^{-1} respectively (Martin et al. 2004a), our search for SiO masers in this object may be slightly easier than is the case in the Sgr dwarf galaxy.

We detected three of the 25 surveyed AGB candidates for the dwarf-galaxy associations. Properties of these candidates are summarized in table 4, which gives the candidate group affiliation (Sgr or CMa candidates), radial velocity in the Galactic Standard of Rest V_{GSR}, $\Lambda_\odot$ and $\beta_\odot$ (the SagDEG coordinates), K and $H-K$, interstellar extinction A_K, estimated distance, IRAS 12 μm flux density, and IRAS name. Here the distance was estimated from the difference between K_c (interstellar- and circumstellar-extinction corrected K magnitude) and a standard $m_K = 6.43$ at the Galactic center (K magnitude for Miras without circumstellar extinction with light variation period of 450 days at 8 kpc; see equation (5) of Glass et al. 1995). Here, the corrected K magnitude, an indicator of distance modulus which is corrected for the interstellar and circumstellar reddening (Fujii et al. 2006), is defined by

$$K_c = K - A_K/E(H-K) \times [(H-K) - (H-K)_0] \quad (1)$$

and we use $A_K/E(H-K) = 1.44$ (Nishiyama et al. 2006), and $(K-H)_0 = 0.5$ (Fujii et al. 2006). Among the surveyed red objects, it turns out that $J14572697+0516034$ is a carbon star (Mauron et al. 2005). Since the associations with the dwarf galaxies are not very certain, we discuss the three SiO detected objects individually.

- $J05475868-3305109$ (IRAS 05461−3306): This is a faint IRAS source with $F_{12} = 2$ Jy. The 2MASS K magnitude is 6.15, suggesting its distance is about 7 kpc. The high radial velocity ($V_{\rm LSR} = 110$ km s^{-1}) and location in the sky ($b = -26.9^\circ$) suggest that this is associated with the CMa dwarf.
- $J08144298-3233047$ (=IRAS 08127−3223): This is a medium bright MSX source G250.9283+01.2198 with $F_C = 9.4$ Jy. Its 2MASS counterpart ($K = 8.44$) has a red $H-K = 2.17$. The interstellar extinction toward this object is quite small ($A_K \sim 0.2$). This object must be an O-rich AGB star undergoing copiously mass-loss. Because of its low galactic latitude ($b = 1.2^\circ$) and small radial velocity ($V_{\rm LSR} = 69$ km s^{-1}), this star is probably a disk star.
- $J19235554-1302029$ (=IRAS 19211−1307): This object is a faint ($F_{12} = 1.1$ Jy) IRAS source at the edge of the Galactic bulge [(l,b)=(24.8°, -13.0°)]. The 2MASS K magnitude ($K = 9.7$) suggests that this star may be located at a distance more than 18 kpc from the Sun, and so could be associated to SagDEG or it's tail, though the radial velocity ($V_{\rm LSR} = -23.0$ km s^{-1}) does not fit the velocity of SagDEG.

Figure 4 shows the velocity–longitude diagram in the SagDEG coordinates for SiO sources; the velocity given is based on the Galactic standard of rest (GSR) by adopting the maginude of the Galactic rotation being 220 km s^{-1}, and the longitude ($\Lambda_\odot$) is measured along the orbital plane of the Sgr dwarf galaxy, with the north pole at $l = 273.8^\circ$ and $b = -13.5^\circ$ (Majewski et al. 2003). By measuring the radial velocities of M giants in the main trail of SagDEG, Majewski et al. (2004) showed that the SagDEG objects fall in a narrow strip crossing at $\Lambda_\odot \sim 65^\circ$ with $V_{GSR} = 0$ km s^{-1}, and that the dispersion of radial velocities of the SagDEG trail is about 10 km s^{-1}. Our candidate star, $J19235554-1302029$ (=IRAS 19211−1307), which is located about 17° below the Sgr orbital plane, deviates from the expected velocity of the tidal stream of SagDEG ($V_{\rm SGR} \sim 160$ km s^{-1}) at this direction by more than 100 km s^{-1}. However, the numerical simulation of the tidal debris (figure 10 of Law et al. 2005) suggests that the trail of SagDEG can produce the $V \sim 50$ km s^{-1} sub-streaming component in this direction; the sub stream is indicated in figure 4 as a thin band between $\Lambda \sim 10^\circ$ and 150° at $V_{\rm SGR}$ range between 0 and 180 km s^{-1}. Though the numerical simulations (Ibata et al. 2001b; Helmi, White 2001) have considerable uncertainty in radial velocities of the sub-stream stars, which were torn from SagDEG in ancient times, the orbits must cross near the present SagDEG position in any simulations. Therefore, the velocity of $V_{\rm GSR} = 67$ km s^{-1} at $\Lambda = 4.2^\circ$ does not exclude the possibility of this object being associated to the Sgr dwarf stream.

Our observation shows that the radial velocity of $J05475868-3305109$, $V_{\rm LSR} = 109$ km s^{-1}, coincides with the above-noted velocity of CMa dwarf (Martin et al. 2004a; Martin et al. 2005). The estimated distance of about 7 kpc for this source (table 4) coincides with the estimated distance of CMa dwarf. These facts suggest an association of this object to the CMa dwarf galaxy. However, $J08144298-3233047$ is unlikely to be associated to CMa dwarf because of its low radial velocity (68.8 km s^{-1}) and low Galactic latitude ($b = 1.2°$).

Even though the association of these objects with dwarf galaxies or their tails is somewhat uncertain, they are still O-rich mass-losing AGB stars located far away from the Sun, and as such are interesting objects. The progenitors of O-rich AGB stars are considered to be more massive than those of C-rich AGB stars, their presence in dwarf galaxies would constrain chemical-evolution and pollution models of dwarf galaxies (e.g., McWilliam & Smecker-Hane 2005).

3.2. A warp signature for the off-plane objects.

It is interesting to check whether the velocity distribution of the off-plane objects ($3° < |b| < 5°$) exhibits any differences from the lower-latitude ($|b| < 3°$) velocity distribution. Upper panel of figure 5 shows a comparison of the velocity distribution between the "on-plane" (lower latitude) and off-plane samples: one from the SiO maser data with $|b| < 3°$ and $0 < l < 45°$ (Deguchi et al. 2004b); the other with $3 < |b| < 5°$ and $0 < l < 45°$ (from the present paper). For the purpose of making the distance cut off as similar as possible for both samples, we have chosen the 127 stars with $F_C > 6.5$ Jy within an area, $0 < l < 45°$ and $|b| < 3°$ for the on-plane sample. At first glance, this diagram gives the impression that the off-plane sample contains a smaller number of objects with $V_{lsr} > 100$ km s^{-1} as compared with those in the on-plane sample. The average of V_{lsr} for the off-plane sample (63 points) is 19.1 ($\pm$60.1) km s^{-1}, while the average of V_{lsr} for the on-plane sample (127 points) is 40.6 ($\pm$59.8) km s^{-1}. This difference of the velocity field between the upper and lower disk samples is valid, because the disk scale height is about 300 pc ($\sim 3°$ at 6 kpc); the off-plane sample ($|b| > 3°$) does not contain many distant disk objects above the disk scale height.

We have made a two-dimensional Kolmogorov-Smirnov (K-S) test (Fasano & Franceschini 1987) for the upper and lower disk samples [for algorithm for the two-sample test, see section 14.7 of Press et al. (1992)]. We found that the null hypothesis of distribution in the longitude-velocity plane for the off-plane sample being the same as distribution of the on-plane sample has a probability of less than 0.1 %. Therefore, the conjecture that the off- and on-plane samples have different velocity distributions is verified with a 99.9 % confidence level. The largest difference in fraction between the two samples is 0.386; this occurs in the upper-left quadrant at the point (l, V_{lsr}) =(13.7°, 30.9 km s^{-1}), which is indicated by a cross in the upper panel of figure 5. Most of the objects on the right side of this point ($l < 14°$) supposedly belong to the Galactic bulge, where the velocity field is different from that of the disk objects. Most of the objects in the left portion ($l > 14$ °) are expected to be disk sources.

The lack of high velocity objects in the off-plane sample appears more strongly for the subsample of the $b < -3°$, $l > 14°$ objects. The lower panel of figure 5 shows a comparison between the velocity distributions of objects with $b < -3°$ and $b > 3°$. Above $l = 14°$, only one object in the $b < -3°$ subsample has $V_{lsr} > 50$ km s^{-1}, while there are 6 objects in the $b > 3°$ subsample with such velocities (though the two-dimensional K-S test for these sets does not give any statistical significance due to the small numbers).

This asymmetry with respect to the Galactic latitude for the off-plane objects can be attributed to the warp of the Galactic disk. Because the warped disk plane is shifted toward positive b in $0 \lesssim l \lesssim 180°$, a shift of the warped disk plane of less than a degree would considerably influence the cut off of the distant objects in off-plane subsamples. Though, in general, the disk warp is considered to appear more strongly for the outer disk samples (Djorgovski & Sosin 1989), it also appears in inner disk samples [for example, see the case for MSX point sources by Vig et al. (2005)]. Figure 6 shows the distribution of sources in the Galactic coordinates and the regression curves for several subsamples. Apparently, in order to obtain the better regression-curve fit, the sample involving distant objects with higher $|b|$ is preferable, so that the upper disk sample in this paper is quite useful to limit the warp parameters. Table 5 lists the bet-fit parameters for three different samples: the on-plane sample ($|b| < 3°$), the whole sample ($|b| < 5°$), and high-velocity ($V_{\rm LSR} > 50$ km s^{-1}) sample. Both the sense of the inclination ($b_0 \sim 2°$) and the shift in the azimuthal angle ($\phi_0 \sim 20$ °) of the warp plane match to those obtained by Vig et al. (2005) analyzing the inner-disk MSX PSC sources.

An alternative explanation of this asymmetric star distribution (especially for the nearby star concentration around $l \sim 23°$ and $b \sim -4°$) could be accretion of a dwarf galaxy debris by the Galaxy. However, the high stellar density of this asymmetric star group in the inner disk virtually excludes such a possibility, though in general it may be hard to distinguish such accretion process from the effect of warp in the outer disk at low star density [for example, arguments in Momany et al. 2006 for the case of CMa over-density].

3.3. A group of stars with unusual velocities: a star stream

We noticed a concentration of three stars with $V_{LSR} < -50$ km s^{-1} in a small area in figure 3 (indicated by filled triangles at lower left); $J19222258-1418050$ (-74.6 km s^{-1}), $J19291840-1916199$ (-68.8 km s^{-1}) $J19310440-1640135$ (-69.4 km s^{-1}). They are concentrated within a few degrees at $(l, b) \sim (21.7°, -15.4°)$. This is quite unusual, because the Galactic rotation at this longitude should give a positive $V_{\rm LSR}$ for most of the objects (except for the stars located very far beyond 15 kpc). These objects are medium bright sources ($F_C = 8$–24 Jy

and $K = 4.2$–5.5), so that their distances are estimated to be less than 7 kpc. We also noticed that some disk maser sources ($|b| < 3^\circ$) occasionally exhibit similarly large negative velocities in the area $15^\circ < l < 30^\circ$; for example, see the SiO and OH l–v diagrams (figure 4) given by Deguchi et al. (2004b). In table 6, we list infrared properties of these objects with radial velocity less than -50 km s^{-1} located in $19^\circ < l < 32^\circ$, giving the IRAS name, the alternative name, Galactic coordinates, $V_{\rm LSR}$, 2MASS K magnitude, $H-K$, and corrected K magnitude K_c, IRAS 12 μm flux density F_{12} and the IRAS color $C_{12}[= log(F_{25}/F_{12})]$.

The positions of these objects are plotted in Galactic coordinates in figure 7. But the CO l–v diagram does not show any feature associated with these velocities in this longitude range (Dame et al. 2001; Kawamura et al. 1999), although there is a distant spiral arm feature spreading at higher velocities [from ($\sim 20^\circ$, 0 km s^{-1}) to ($\sim 40^\circ$, -50 km s^{-1}] (due to the 15 kpc arm). We also do not find any negative-velocity SiO maser sources with $V_{\rm LSR} < -50$ km s^{-1} up to the longitude $l = 50^\circ$, where distant objects obeying the Galactic rotation start to show negative $V_{\rm LSR}$ (for example see figure 8 of Nakashima, Deguchi 2003). Note that the radial velocities of these stars, if motion of the Local Standard of Rest (220 km s^{-1}) about the Galactic center is subtracted (i.e., velocities in the GSR), are quite small (~ 20 km s^{-1}), suggesting that these stars are moving perpendicularly to the line of sight with a high speed.

The origin of this negative velocity group is not clear. We have several conjectures. One is that they are a part of the radial outward stellar motion, which is produced by the dynamical effect of the bulge bar. According to an analysis of Hipparcos data made by Feast & Whitelock (2000), a stream of short-period Mira stars is observed at negative velocities (~ -75 km s^{-1}) toward the bulge and some of these extend beyond the solar circle. The negative-velocity streaming of these stars spreads in a large scale toward the bulge. The feature we observe, especially around $l \sim 30^\circ$ might be a part of this large-scale outward star flow; the concentration around $(l, b) \sim (22^\circ, -15^\circ)$ may be a stochastic effect.

An alternative conjecture is that the velocity structure is a manifestation of a star stream crossing in the Galactic disk (for example, see Navarro et al. 2004). The broken line in figure 7 indicates a linear least-squares fit to the positions of the negative velocity objects. We found that this regression line passes within 0.1° of NGC 6712. This globular cluster has $V_{\rm LSR} = -92$ km s^{-1} (Harris 1996), that is close to the average velocity of these objects (-69.3 km s^{-1}) if the uncertainty of optical radial velocity measurements of globular-cluster members (of about 20 km s^{-1}) is factored in (Matsunaga et al. 2005). The other 2 nearby globular clusters have somewhat similar radial velocities ($V_{\rm LSR} = -53.9$ km s^{-1} and -44.9 km s^{-1} for Pal 11 and NGC 6749, respectively) except for NGC 6760 ($V_{\rm LSR} = 10.9$ km s^{-1}). It is possible that these globular clusters are fossil remnants of the same dwarf galaxy plunging into the dense inner disk of the Galaxy. In fact, de Marchi et al. (1999) found evidence of tidal disruption of NGC 6712. Paltrinieri et al. (2001) found about one hundred blue stragglers in the same globular cluster. In the core of globular clusters, it is possible to generate the antecedents of AGB stars by main-sequence mergers (Matsunaga et al. 2005; Andronov et al. 2006), and later they can escape out from the original globular cluster by tidal interactions. Because primordial low-mass metal-poor stars in aged globular clusters ($M < 1 M_\odot$) cannot be evolved to SiO maser stars with large mass-loss rates at the AGB phase, only larger mass stars such as merger antecedents can be sources of maser stars in globular clusters or dwarf galaxies. Although, at present, we do not have any other strong evidence of existence of the dwarf galaxy or it's tidal tail in this direction, the presence of a star stream remains to be an interesting speculation.

4. Summary

We surveyed 277 2MASS/MSX or IRAS sources off the Galactic plane and obtained more than one hundred new detections in the SiO maser lines. Two of these SiO sources are associated with very faint infrared objects, and are likely to be associated with the Sgr or CMa dwarf galaxies. We also found a clear signature of a warp of the Galactic disk in the off-plane ($|b| > 3^\circ$) sample. Furthermore, we found an interesting group of O-rich AGB stars at $(l, b) \sim (22^\circ, -15^\circ)$, which do not follow the Galactic rotation. This may suggest the presence of a stream of stars penetrating the Galactic disk, whose origin is not clear.

Authors thank Dr. B. M. Lewis for the useful comments and kind advices on English. One of authors (A.W.) aknowledges National Astronomical Observatory of Japan for approving him a short-term visiting fellowship in 2003. This research made use of the SIMBAD and VizieR databases operated at CDS, Strasbourg, France, as well as use of data products from Two Micron All Sky Survey, which is a joint project of the University of Massachusetts and Infrared Processing and Analysis Center/California Institute of Technology, funded by the National Aeronautics and Space Administration and National Science foundation, and from the Midcourse Space Experiment at NASA/ IPAC Infrared Science Archive, which is operated by the Jet Propulsion Laboratory, California Institute of Technology, under contract with the National Aeronautics and Space Administration.

Appendix. Individual Objects

The SiO maser spectra for the newly detected objects are shown in Figure 8a–8g. We discuss here interesting objects individually.

- *J*06353168−0109256 (IRAS 06329−0106): This object has a radial velocity 100.4 km s^{-1} at $l = 212^\circ$, which is considerably large if compared with the Galactic rotational velocity (see the lower panel of

figure 3). The SiO masers were detected first by Jiang et al. (1996). This object is a bright infrared source ($K = 3.7$ and $F_{12} = 18.8$ Jy) with IRAS LRS class 29 (silicate emission ; Olnon et al. 1986), suggesting a distance of a few kpc. It is unlikely that this is associated to CMa dwarf or its tail.

- *J*17572314−1802456 (IRAS 17544−1802): This object is denoted as LDN 292, a dark Nebula, in the SIMBAD database. However, the detection of SiO masers secures this object as an AGB star, which is consistent with its IRAS LRS class of 29 (silicate emission). The 2MASS images exhibit a faint nebulosity of size of about 30″ toward this bright (K=3.546) object.
- *J*17001324−1037003 (IRAS 16574−1032 =V2207 Oph =IRC −10355): This is a strong IRAS source with $F_{12} = 89.6$ Jy and LRS class of 28 (silicate emission). Previous searches for OH 1612 MHz and H_2O 22 GHz emission were negative (te Lintel-Hekkert et al. 1991; Lewis 1997). Nyman et al. (1992) included this object in the list of tentative detections by the CO $J = 1$–0 line, but the radial velocity was not given. NIR light variations have been detected (Lockwood et al. 1985). The detection of strong SiO masers at $V_{lsr} = -42.0$ km s^{-1} confirms that this is a mass-losing AGB star.
- *J*17335931−2659216 (IRAS 17308−2657): This object has a large negative radial velocity of −261 km s^{-1}. Its position $[(l, b) = (0.3°, +3.2°)]$ and infrared flux densities ($F_C = 7.7$ Jy and $K = 7.9$) indicate that this is a star in the Galactic bulge. Large negative radial velocities are common for bulge stars in the x_1 orbit family (Fujii et al. 2006).
- *J*17415458−2047055 (IRAS 17389−2045): This is a strong infrared source with $F_{12} = 66.0$ Jy and LRS class of 28 (silicate emission). OH 1612 MHz and 1665/67 MHz lines have been detected (Le Squeren et al. 1992; David et al. 1993) at $V_{lsr} = 13.8$ and 47.5 km s^{-1}, the mean velocity being consistent with the SiO detection at $V_{lsr} = 31.3$ km s^{-1}. This object was included in the relatively small number of the AGB stars sampled by IRTS; from infrared spectra between 1–5 μm, the distance was estimated to be about 1 kpc (Le Bertre et al. 2001).
- *J*18085198−2616210 (IRAS 18057−2616): This is a strong infrared source with F_{12}=59 Jy with LRS class of 26 (silicate emission). An OH 1612 MHz maser was detected at $V_{\rm lsr} = -7.7$ and 29.7 km s^{-1} (te Lintel-Hekkert et al. 1991), the mean velocity being consistent with SiO radial velocity of 11.1 km s^{-1}.
- *J*23584412−3926599 (=RR Phe) : Though it is a well-known optical/NIR variable star with a period of 427 days (Jura et al. 1993) located close to the South Galactic pole (b=−73.5°), it was not recorded in the IRAS catalog because of its position in the IRAS gap and had been neglected. The MSX out-of-plane survey found this object as a strong MIR source with $F_C = 289$ Jy. We detected relatively strong SiO maser emission at $V_{\rm lsr}$=18 km s^{-1}. No previous OH or H_2O maser observation was found for this star.

References

Andronov, N., Pinsonneault, M. H., Terndrup, D. M. 2006, ApJ, 646, 1160

Bellazzini, M., Ibata, R., Monaco, L., Martin, N., Irwin, M. J., & Lewis, G. F. 2004, MNRAS, 354, 1263

Binney, J. 2001, ASP Conf. Ser., 228, 269

Dame, T. M., Hartmann, D., & Thaddeus, P. 2001, ApJ, 547, 792

David, P., Le Squeren, A. M., Sivagnanam, P., Braz, M. A.1993, A&AS, 98, 245

de Marchi, G., Leibundgut, B., Paresce, F., & Pulone, L. 1999, A&A, 343, L9

Deguchi, S., Fujii, T., Izumiura, H., Matsumoto, S., Nakada, Y., Wood, P. R., & Yamamura, I. 1999, PASJ, 51, 355

Deguchi, S., Fujii, T., Izumiura, H., Kameya, O., Nakada, Y., Nakashima, J., Ootsubo, T., & Ukita, N. 2000a, ApJS, 128, 571

Deguchi, S., Fujii, T., Izumiura, H., Kameya, O., S. Nakada, Y., & Nakashima, J. 2000b, ApJS, 130, 351

Deguchi, S., Nakashima, J., & Balasubramanyam, R. 2004, PASJ, 53, 305

Deguchi, S., et al. 2004a, PASJ, 56, 261

Deguchi, S., et al. 2004b, PASJ, 56, 765

Deguchi, S., Nakashima, J., Kwok, S., & Konig, N. 2007, ApJ, (submitted)

Djorgovski, S. & Sosin, C. 1989, ApJ, 341, L13

Eder, J., Lewis, B. M., & Terzian, Y. 1988, ApJS, 66, 183

Egan M.P., Price S.D., Kraemer K.E., Mizuno D.R., Carey S.J., Wright C.O., Engelke C.W., Cohen M., Gugliotti G. M. 2003, Air Force Research Laboratory Technical Report AFRL-VS-TR-2003-1589 available at *http://vizier.nao.ac.jp/viz-bin/VizieR?-source=V/114*

Fasano, G. & Franceschini, A. 1987, MNRAS, 225, 155

Feast, M. W. & Whitelock, P. A. 2000, MNRAS, 317, 460

Fujii, T., Deguchi, S., Ita, Y., Izumiura, H., Kameya, O., Miyazaki, A., Nakada, Y. 2006, PASJ, 58, 529

Glass, I. S., Whitelock, P. A., Cathcpole, R. M. & Feast, M. W. 1995, MNRAS 273, 383

Harris, W. E. 1996, AJ, 112, 1487

Helmi, A. & White, S. D. M. 2001, MNRAS, 323, 529

Ibata, R. A., Gilmore, G., & Irwin, M. J. 1994, Nature 370, 194

Ibata, R., Irwin, M., Lewis, G., & Stolte, A. 2001a, ApJ, 547, L133

Ibata, R., Lewis, G., Irwin, M., Totten, E., & Quinn, T. 2001b, ApJ, 551, 294

Iben, I., Jr. 1981, ApJ, 246, 278

Ita, Y., Deguchi, S., Fujii, T., Kameya, O., Miyoshi, M., Nakada, Y., Nakashima, J., & Parthasarathy, M. 2001, A&A, 376, 112

Izumiura, H., Deguchi, S., Hashimoto, O., Nakada, Y., Onaka, T., Ono, T., Ukita, N., & Yamamura, I. 1995, ApJ, 453, 837

Jiang, B. W., Deguchi, S., Yamamura, I., Nakada, Y., Cho, S. H., & Yamagata, T. 1996, ApJS, 106, 463

Jura, M., Yamamoto, A., & Kleinmann, S. G. 1993, ApJ, 413, 298

Kawamura, A., Onishi, T., Mizuno, A., Ogawa, H., & Fukui, Y. 1999, PASJ, 51, 851

Kobulnicky, H. A., Monson, A. J., Buckalew, B. A. et al. 2005, AJ, 129, 239
Law, D. R., Johnston, K. V., & Majewski, S. R. 2005, ApJ, 619, 807
Le Bertre, T., Matsuura, M., Winters, J. M., Murakami, H., Yamamura, I., Freund, M., & Tanaka, M. 2001, A&A, 376, 997
Le Squeren, A. M., Sivagnanam, P., Dennefeld, M., David, P. 1992, A&A, 254, 133
Lewis, B. M. 1997, AJ, 114, 1602
Lockwood, G. W. 1985, ApJS, 58, 167
Majewski, S. R., Skrutskie, M. F., Weinberg, M. D., & Ostheimer, J. C. 2003, ApJ, 599, 1082
Majewski , S. R. et al. 2004, ApJ, 128, 245
Martin, N. F., Ibata, R. A., Conn, B. C., Lewis, G. F., Bellazzini, M., Irwin, M. J., & McConnachie, A. W. 2004, MNRAS, 355, L33
Martin, N. F., Ibata, R. A., Bellazzini, M., Irwin, M. J., Lewis, G. F., & Dehnen, W. 2004, MNRAS, 348, 12
Martin, N. F., Ibata, R. A., Conn, B. C., Lewis, G. F., Bellazzini, M., & Irwin, M. J. 2005, MNRAS, 362, 906
Matsunaga, N., Deguchi, S., Ita, Y., Tanabe, T., & Nakada, Y. 2005, PASJ, 57, L1
Mauron, N., Kendall, T. R., & Gigoyan, K. 2005, A&A, 438, 867
McWilliam, A. & Smecker-Hane, T. A. 2005, ASPC, 336, 221 Edited by Thomas G. Barnes III and Frank N. Bash, (Astronomical Society of the Pacific; San Francisco)
Messineo, M., Habing, H. J., Sjouwerman, L. O., Omont, A., & Menten, K. M. 2002, A&A, 393, 115
Momany, Y., Zaggia, S., Gilmore, G., Piotto, G., Carraro, G., Bedin, L. R., & de Angeli, F. 2006, A&A, 451, 515
Navarro, J. F., Helmi, A., & Freeman, K. C. 2004, ApJL, 601, L43
Nakashima, J., & Deguchi, S. 2003, PASJ, 55, 203
Nishiyama, S., Nagata, T., Kusakabe, N., et al. 2006, ApJ, 638, 839
Nyman, L.-Å. Booth, R. S. Carlström, U. Habing, H. J. Heske, A. Sahai, R. Stark, R. van der Veen, W. E. C. J., & Winnberg, A.1992, A&AS, 93, 121
Nyman, L.-Å., Hall, P.J., & Olofsson, H. 1998, A&AS, 127, 185
Olnon, F. M., Raimond, E. R., & IRAS Science team, 1986, A&AS, 65, 607
Paltrinieri, B., Ferraro, F., Paresce, F., & de Marchi, G. 2001, AJ, 121, 3114
Press, W. H., Flannery, B. P., Teukolsky, S. A., & Vetterling, W. T. 1992, "Nemerical Recipe in C" (Cambridge University Press; Cambridge)
Sato, S. 2002, The Proceedings of the IAU 8th Asian-Pacific Regional Meeting, Vol. II, Ed. by S. Ikeuchi, J. Hearnshaw, & T. Hanawa, the Astronomical Society of Japan, p. 27
Sevenster, M. N., Chapman, J. M., Habing, H. J., Killeen, N. E. B., & Lindqvist, M. 1997, A&AS, 122, 79
Sevenster, M. N., van Langevelde, H. J., Moody, R. A., Chapman, J. M., Habing, H. J., & Killeen, N. E. B. 2001, A&A, 366, 481
te Lintel-Hekkert, P., Caswell, J. L., Habing, H. J., Haynes, R. F., & Norris, R. P. 1991, A&AS, 90, 327
van Loon, J. T., Zijlstra, A. A., Bujarrabal, V., & Nyman, L.-Å. 1996, A&A, 306, L29
Vig, S., Ghosh, S. K., & Ojha, D. K. 2005, A&A, 436, 867
Wood, P. R.,Whiteark, S. M., Hughes. Sm. M. G, Bessel, M. S., Gardne. F. F., Hyland, A. R. 1992, ApJ, 397, 552
Yanny, B., Newberg, H.J., Grebel, E. K., Kent, S., et al. 2003, ApJ, 588, 824

Table 1. SiO detections.

2MASS name	SiO $J=1$–0 $v=1$				SiO $J=1$–0 $v=2$				Obs. date	$V_{\rm ave}$
	$V_{\rm peak}$ (km s^{-1})	$T_{\rm peak}$ (K)	Flux (K km s^{-1})	RMS (K)	$V_{\rm peak}$ (km s^{-1})	$T_{\rm peak}$ (K)	Flux (K km s^{-1})	RMS (K)	(yymmdd.d)	(km s^{-1})
*J*02160009−2031108	4.1	0.362	0.722	0.072	−1.3	0.950	1.515	0.096	030516.5	1.4
*J*03055291+5420538	−28.6	0.249	0.387	0.043	−28.0	0.367	0.424	0.049	990516.5	−28.3
*J*05475868−3305109	110.8	0.114	0.471	0.030	—	—	—	0.039	040226.8	110.8
*J*06215148−0350416†	−7.3	1.541	5.152	0.053	−7.3	1.456	4.861	0.107	000115.9	−7.3
*J*06353168−0109256†	100.1	1.103	2.336	0.094	100.7	0.932	2.070	0.101	000407.6	100.4
*J*06421530−0939442†	26.4	3.954	10.679	0.100	26.4	4.503	10.071	0.123	000407.7	26.4
*J*06425082−0141061†	17.8	0.297	0.717	0.060	18.3	0.543	1.128	0.068	000116.9	18.0
*J*07072736−2538440	84.9	1.006	5.406	0.076	85.1	0.835	4.324	0.079	000116.9	85.0
*J*07112217−0129391	59.8	0.270	1.000	0.042	61.5	0.276	0.472	0.049	000116.0	60.7
*J*07172817−2417135†	59.9	0.588	1.404	0.083	59.6	0.881	2.618	0.108	000407.7	59.7
*J*07201954−1320137‡	59.1	0.901	2.773	0.139	61.4	1.054	4.462	0.158	000115.0	60.3
*J*07221634−1852159†	29.0	1.042	2.635	0.109	29.2	0.945	2.774	0.114	000405.8	29.1
*J*07463415−3218165	26.3	6.101	43.768	0.076	31.5	5.687	20.633	0.095	000408.8	28.9
*J*07494088−3933293	94.7	1.871	6.505	0.123	94.7	1.603	6.500	0.138	000117.0	94.7
*J*07514440−3519526	51.3	0.286	1.502	0.048	52.0	0.278	1.228	0.062	000116.0	51.7
*J*08104779−3520442	72.9	1.600	2.903	0.149	72.6	1.822	3.224	0.166	000406.7	72.8
*J*08144298−3233047	68.6	0.173	0.692	0.037	69.0	0.169	0.368	0.046	040115.9	68.8
*J*08400691−0813472	31.7	0.660	4.482	0.068	28.1	0.605	3.489	0.089	030516.6	29.9
*J*09045184−2810357§	86.1	0.216	0.729	0.061	91.2	0.220	0.505	0.072	000406.8	88.7
*J*09220626−2934129	14.8	0.506	2.065	0.068	15.0	0.655	2.753	0.078	000408.7	14.9
*J*10255751−0730506	52.0	0.904	3.282	0.107	54.5	0.403	0.541	0.100	040507.8	53.2
*J*10533744+1342544	46.7	2.310	8.704	0.099	45.7	1.613	6.075	0.143	040507.8	46.2
*J*11414026+3828293	−56.3	0.240	0.225	0.039	—	—	—	0.051	040510.9	−56.3
*J*14280928−3300034	−18.0	2.364	9.758	0.099	−18.2	1.390	8.593	0.128	040512.0	−18.1
*J*15331652−1519350	−36.0	0.334	0.706	0.066	−36.2	0.783	1.065	0.086	050524.9	−36.1
*J*15332161−2711031	9.9	1.507	2.299	0.153	9.7	1.920	4.245	0.194	050524.9	9.8
*J*15463127−2107395	−56.8	0.717	1.962	0.092	—	—	—	0.106	050525.0	−56.8
*J*16015727−3846475	−83.9	1.108	2.269	0.132	−83.7	1.815	2.547	0.159	040422.1	−83.8
*J*16055729−2747309	46.9	0.702	1.093	0.069	47.3	0.553	0.921	0.093	040421.1	47.1
*J*16203527−3209370	−62.4	0.881	3.333	0.099	−62.7	0.855	2.748	0.131	040512.0	−62.6
*J*16324854−2623062	−17.5	0.215	0.850	0.047	—	—	—	0.059	050524.0	−17.5
*J*16395065−2406083	−9.0	0.308	0.626	0.072	−10.2	0.444	0.922	0.091	040518.0	−9.6
*J*16521293−1257016	−15.4	3.034	8.802	0.094	−8.1	1.481	7.972	0.121	040329.1	−11.7
*J*16543110−0733376	29.3	0.092	0.154	0.038	32.0	0.157	0.647	0.048	040330.3	30.7
*J*17001324−1037003	−42.0	4.808	11.724	0.103	−42.0	10.252	19.586	0.133	040329.1	−42.0
*J*17030696−2033255	63.2	1.866	9.331	0.100	69.6	2.493	13.512	0.135	040226.2	66.4
*J*17061081−1028590	2.1	0.859	2.712	0.082	1.4	1.281	3.382	0.101	040330.2	1.8
*J*17121537−1637006	43.9	0.292	1.321	0.055	41.7	0.256	1.011	0.069	040418.1	42.8
*J*17272810−3047542	−19.2	0.315	0.660	0.060	−14.3	0.163	0.240	0.078	040508.1	−16.7
*J*17334246−2633545	19.6	0.198	0.498	0.049	20.8	0.231	0.305	0.061	050524.0	20.2
*J*17335931−2659216	−260.8	0.312	1.312	0.075	−262.2	0.424	1.533	0.087	050529.9	−261.5
*J*17365144−2516262	22.1	0.398	1.097	0.081	21.3	0.562	1.262	0.100	040226.2	21.7
*J*17365757−2418066	−61.8	0.635	1.952	0.076	−62.0	0.584	1.611	0.096	050526.0	−61.9
*J*17373815−2557269	−58.9	0.365	1.557	0.073	−59.3	0.323	0.463	0.094	050528.0	−59.1
*J*17394268−2134239	32.7	0.172	0.290	0.050	29.8	0.247	0.395	0.065	040419.1	31.3
*J*17415458−2047055	37.3	2.741	12.531	0.107	25.2	3.467	14.630	0.145	040226.2	31.3
*J*17431835−2109031	30.0	0.364	1.254	0.068	36.0	0.320	1.110	0.092	050526.0	33.0
*J*17441045−2215239	79.0	0.268	0.180	0.062	80.0	0.300	0.719	0.080	040517.1	79.5
*J*17454035−2223291	−14.3	2.167	7.818	0.130	−14.3	1.576	4.830	0.165	040511.0	−14.3
*J*17472779−2058089	22.3	0.306	1.230	0.057	21.9	0.361	1.607	0.074	040419.2	22.1
*J*17532342−1902545	−6.0	0.162	0.125	0.045	−4.9	0.246	0.437	0.057	050526.0	−5.4
*J*17551128−1852359	94.3	0.900	3.248	0.106	92.9	0.458	1.286	0.136	050529.0	93.6
*J*17555714−1531531	48.2	0.666	2.509	0.080	49.7	0.434	1.766	0.099	040517.0	48.9

Table 1. (Continued.)

2MASS name	SiO $J=1$–0 $v=1$				SiO $J=1$–0 $v=2$				Obs. date	$V_{\rm ave}$
	$V_{\rm peak}$ (km s^{-1})	$T_{\rm peak}$ (K)	Flux (K km s^{-1})	RMS (K)	$V_{\rm peak}$ (km s^{-1})	$T_{\rm peak}$ (K)	Flux (K km s^{-1})	RMS (K)	(yymmdd.d)	(km s^{-1})
J17572314−1802456	2.8	1.113	5.881	0.081	2.8	1.496	7.212	0.106	040514.1	2.8
J17573605−1825517	−29.8	0.530	1.213	0.100	−29.7	0.860	2.028	0.136	050529.0	−29.8
J17593665−1735346	97.8	0.358	0.452	0.070	92.6	0.317	0.589	0.085	050529.0	95.2
J18001195−2947267	32.6	1.056	2.793	0.108	32.5	1.389	2.602	0.140	040422.2	32.5
J18083501−2609029	−7.7	0.236	0.818	0.056	−10.2	0.239	0.598	0.075	050530.0	−9.0
J18085198−2616210	10.6	4.219	20.777	0.122	11.6	1.971	12.815	0.159	040514.1	11.1
J18100465−2559418	−43.0	2.439	7.600	0.194	−42.9	2.365	5.014	0.231	050526.1	−42.9
J18111148−2705565	−5.8	1.076	3.662	0.161	−4.9	1.186	4.205	0.187	050529.0	−5.3
J18121417−2243588	77.0	0.208	0.552	0.045	—	—	—	0.065	040508.2	77.0
J18125638−2434279	33.4	0.911	2.723	0.092	33.9	0.859	2.180	0.119	040422.2	33.6
J18130340−2451495	1.8	0.411	0.283	0.096	2.2	1.319	3.927	0.127	040423.2	2.0
J18135525−1047054	43.2	1.096	3.565	0.100	43.1	0.996	2.751	0.129	040419.2	43.1
J18144245−2355098	44.4	0.372	0.851	0.072	43.9	0.428	0.729	0.095	050527.1	44.1
J18182505−0825596	-12.1	1.807	3.343	0.145	-12.2	1.700	3.056	0.130	060421.2	-12.1
J18183625−0812320	116.1	0.814	2.062	0.124	116.2	1.080	2.207	0.123	040516.0	116.2
J18192924−2302044	22.5	0.268	1.271	0.070	20.4	0.395	0.650	0.088	050311.2	21.4
J18194627−2352057	41.6	1.138	2.844	0.101	41.2	0.776	1.648	0.130	050311.2	41.4
J18202016−2303504	8.0	1.570	3.725	0.115	9.4	0.792	0.890	0.152	040423.2	8.7
J18223070−2041121	99.0	1.296	4.522	0.123	99.1	1.390	4.047	0.121	060419.2	99.1
J18231258−2100114	71.0	0.580	2.170	0.074	71.5	0.491	1.577	0.097	050311.2	71.2
J18252822−2205007	17.6	0.301	1.297	0.059	22.1	0.351	1.009	0.071	050311.3	19.9
J18253701−2153267	−54.5	0.406	1.698	0.063	−53.0	0.278	1.605	0.071	050214.4	−53.7
J18263203−0443370	86.6	0.557	2.750	0.068	87.6	0.486	2.128	0.091	040514.1	87.1
J18264589−1925293	139.0	0.293	0.858	0.061	139.1	0.285	0.971	0.062	060419.2	139.1
J18270303−2014544	39.9	0.959	4.801	0.102	40.1	0.710	3.055	0.102	060419.2	40.0
J18272475−0357552	15.7	1.266	4.036	0.082	15.2	1.411	3.983	0.105	040514.1	15.5
J18272645−0422462	64.2	0.697	2.306	0.094	62.2	0.391	2.019	0.090	060411.2	63.2
J18281254−0417486	−15.5	0.680	1.922	0.115	−15.3	0.883	1.719	0.113	060411.3	-15.4
J18343099−0025046	63.4	0.477	1.515	0.063	61.9	0.504	1.259	0.076	040517.0	62.6
J18350137−1545026	−9.8	1.185	4.993	0.144	−9.5	1.263	5.950	0.165	040517.0	−9.6
J18364919−1351561	−36.9	1.917	5.108	0.120	−38.3	0.924	3.433	0.154	040517.1	−37.6
J18380663+0229591	95.8	0.530	1.854	0.079	97.3	0.295	1.000	0.081	060411.2	96.6
J18393585−1231005	12.1	0.990	3.342	0.127	9.3	0.966	3.010	0.152	040517.1	10.7
J18425242−1210401	27.1	1.056	3.907	0.126	27.0	2.138	6.556	0.161	040517.1	27.0
J18451857−1010551	15.4	0.616	3.564	0.106	19.0	0.550	2.460	0.131	040517.0	17.2
J18454730+0527211	74.1	0.516	0.987	0.151	74.5	0.648	1.272	0.187	040516.0	74.3
J18455342−1203361	20.0	0.518	1.158	0.086	20.5	0.539	1.843	0.106	040517.1	20.3
J18475335−0919102	−49.4	0.442	1.614	0.073	−49.5	0.677	1.251	0.091	040420.2	−49.5
J18475454−0821287	7.6	1.452	3.376	0.129	7.9	1.615	2.256	0.163	040517.1	7.7
J18484390−1141297	27.2	0.822	2.838	0.143	27.5	0.913	1.371	0.173	040517.1	27.3
J18495125−0939299	−7.6	0.711	2.431	0.124	−8.2	0.874	2.484	0.156	040517.2	−7.9
J18500474+0559286	50.5	0.356	0.867	0.069	50.5	0.280	0.346	0.090	040516.1	50.5
J18503766+0409088	58.3	0.268	0.227	0.067	57.3	0.275	0.807	0.080	040330.4	57.8
J18532358−2620122	46.6	0.717	1.680	0.107	46.4	1.015	1.856	0.123	040420.2	46.5
J18541840−0648564	−21.0	1.299	3.704	0.095	−20.6	0.720	2.899	0.119	040517.2	−20.8
J18542609+1018031	29.6	0.435	0.511	0.078	—	—	—	0.079	060416.3	29.6
J18551284+1041470	−51.4	0.414	1.860	0.109	−55.0	0.903	2.675	0.151	050529.1	−53.2
J18590806+1051001	1.5	0.334	1.308	0.077	−0.5	0.452	1.822	0.093	040420.1	0.5
J19012350−2726106	85.6	0.287	0.882	0.050	84.1	0.303	0.827	0.061	040420.2	84.8
J19012574−0529398	88.4	0.884	2.476	0.098	87.8	0.709	1.229	0.118	040420.1	88.1
J19014986−1910383	18.8	0.823	2.576	0.105	19.0	1.012	2.033	0.140	040512.2	18.9
J19022521−2037492	90.1	0.252	0.608	0.045	92.7	0.181	0.653	0.061	030517.2	91.4
J19040549−0320389	39.4	0.321	0.448	0.072	39.3	0.339	0.740	0.062	060421.2	39.3

Table 1. (Continued.)

2MASS name	SiO $J=1$–0 $v=1$				SiO $J=1$–0 $v=2$				Obs. date	$V_{\rm ave}$
	$V_{\rm peak}$ (km s^{-1})	$T_{\rm peak}$ (K)	Flux (K km s^{-1})	RMS (K)	$V_{\rm peak}$ (km s^{-1})	$T_{\rm peak}$ (K)	Flux (K km s^{-1})	RMS (K)	(yymmdd.d)	(km s^{-1})
J19061474+0002251	49.3	2.532	7.178	0.112	49.2	2.198	6.476	0.150	050530.1	49.3
J19085920−1510032	51.6	0.441	2.522	0.068	52.4	0.357	1.495	0.090	030516.2	52.0
J19123923−2341470	62.0	0.627	1.114	0.108	61.5	0.790	0.815	0.134	030516.2	61.7
J19173939−1322488	49.8	0.866	2.700	0.102	49.7	0.413	1.145	0.135	030516.2	49.8
J19221604+0506593	−33.2	0.325	1.630	0.073	−34.3	0.543	1.348	0.099	050530.1	−33.7
J19222258−1418050[♭]	−74.6	0.322	1.452	0.065	−74.6	0.417	0.292	0.091	040508.2	−74.6
J19235554−1302029	−20.7	0.124	0.151	0.027	−25.3	0.190	0.435	0.037	030517.2	−23.0
J19291840−1916199	−69.3	0.386	0.721	0.078	−68.4	0.465	1.447	0.107	040512.2	−68.8
J19302125−1232535	140.9	0.186	0.374	0.055	140.5	0.435	0.615	0.064	030518.2	140.7
J19310440−1640135	−69.5	1.494	5.181	0.065	−69.3	1.014	2.547	0.084	050214.4	−69.4
J19465644−0822022	—	—	—	0.045	22.0	0.269	0.512	0.065	040508.2	22.0
J21582555+6343270	−61.9	2.362	20.436	0.063	−62.5	1.463	11.926	0.081	040509.3	−62.2
J23584412−3926599	18.4	4.281	10.310	0.156	18.3	4.783	9.779	0.200	040508.4	18.4

[†] detected previously by Jiang et al. (1996).
[‡] detected previously by Nyman et al. (1998).
[§] the SiO $J=2$–1 $v=1$ emission detected previously by Deguchi et al. (2001).
[♭] detected previously by Ita et al. (2001).

Table 2. Negative results.

name	RMS($v=1$) (K)	RMS($v=2$) (K)	Obsdate (yymmdd.d)
*J*01015839+5759482	0.053	0.059	990515.5
*J*02005614+0945356	0.037	0.027	030516.4
*J*02151393+5613030	0.069	0.074	990515.5
*J*02300585+4007038	0.039	0.030	030516.3
*J*02311288+6340198	0.102	0.213	990515.6
*J*03133515+5948036	0.049	0.046	990517.5
*J*03230583+5652435	0.043	0.040	990517.6
*J*03275901+6044553	0.038	0.031	990516.6
*J*03404991+4941534	0.054	0.044	990519.5
*J*03482812+1657032	0.030	0.022	030517.5
*J*03552337+1133437	0.035	0.027	030516.5
*J*03563582+5720279	0.047	0.039	990516.6
*J*03591178+4413103	0.048	0.045	990517.6
*J*03595596+0919044	0.037	0.027	030517.4
*J*04432934+3432189	0.053	0.046	990517.6
*J*04501343+3007449	0.062	0.053	990517.6
*J*05233987+3230157	0.105	0.086	990514.7
*J*05301817+2022024	0.076	0.070	990517.7
*J*05434967+3242061	0.110	0.093	990514.6
*J*05481570+2001593	0.062	0.056	990520.6
*J*05514643+3522189	0.069	0.056	990521.6
*J*06092550−0938492	0.067	0.060	000116.9
*J*06181637−1702347	0.045	0.041	000115.9
*J*06195821−1038146	0.058	0.049	000405.7
*J*06204380−0433270	0.066	0.064	000114.9
*J*06243845−1753432	0.071	0.069	000116.9
*J*06265390−1015349	0.057	0.050	000406.6
*J*06342805−0503427	0.063	0.056	000405.7
*J*06370162−0127018	0.047	0.039	000407.6
*J*06413391−0806289	0.035	0.029	000115.9
*J*06440823−1320089	0.045	0.037	000408.6
*J*06470984−0358461	0.063	0.058	000116.9
*J*06472497+0813588	0.043	0.037	990516.6
*J*06474716+1636326	0.052	0.043	990521.6
*J*06505251−0004235	0.040	0.035	000115.9
*J*06513922−2123303	0.028	0.040	040226.8
*J*06522047−0328407	0.042	0.034	000408.7
*J*06530149−0453501	0.066	0.053	000407.7
*J*06551745−1647526	0.070	0.064	000116.9
*J*06552346−2122258	0.033	0.040	040113.0
*J*07065685−1109395	0.065	0.063	000116.9
*J*07074938−1044059	0.090	0.092	000114.9
*J*07122348−0124521	0.044	0.037	000405.7
*J*07132317−2752580	0.129	0.132	000115.0
*J*07132320−0718336	0.072	0.063	000405.8
*J*07143791−2513019	0.024	0.029	040226.8
*J*07184575−2123318	0.066	0.058	000407.7
*J*07243912−0437541	0.069	0.057	000407.7
*J*07251926−1121214	0.032	0.041	040112.9
*J*07291120−2610322	0.066	0.058	000408.8
*J*07321227−2147136	0.093	0.077	000405.8
*J*07364088−1018431	0.046	0.035	000408.7
*J*07394181−2834172	0.148	0.131	000405.8
*J*07445699−1541500	0.069	0.073	000115.0
*J*07454092−1854291	0.064	0.051	000406.7

Table 2. (Continued.)

name	RMS($v=1$) (K)	RMS($v=2$) (K)	Obsdate (yymmdd.d)
*J*07454503−3619503	0.101	0.080	000406.8
*J*07493363−2546454	0.053	0.045	000406.7
*J*07493726−3820439	0.044	0.053	040114.9
*J*07495786−3654299	0.150	0.131	000406.8
*J*07521749−0329044	0.065	0.048	030517.6
*J*07531683−1129311	0.069	0.057	000406.6
*J*07554019−2838544	0.125	0.101	000408.7
*J*07585240−0122349	0.044	0.058	040114.8
*J*08003235−3559477	0.058	0.058	040114.0
*J*08004940−3655221	0.167	0.153	000117.1
*J*08020499−3811522	0.139	0.133	000117.1
*J*08031918−3138009	0.072	0.058	000408.8
*J*08043072−0307483	0.064	0.053	000406.7
*J*08102688−3914152	0.121	0.117	000117.0
*J*08105244−3515260	0.080	0.068	000406.7
*J*08121082−2343485	0.061	0.050	000407.8
*J*08141230−4142291	0.077	0.072	000117.0
*J*08160288−3536539	0.047	0.066	040226.8
*J*08191830−2144143	0.062	0.050	000407.8
*J*08200755−2616323	0.052	0.041	000408.7
*J*08214679−1346410	0.051	0.075	040226.9
*J*08221114−2537546	0.077	0.064	000407.8
*J*08255320−3333507	0.056	0.048	000406.8
*J*08293488−3836214	0.126	0.124	000117.0
*J*08333853−3707051	0.057	0.073	040226.8
*J*08362321−4057172	0.094	0.083	000407.8
*J*08392931−4013441	0.167	0.155	000117.0
*J*08451851+1420341	0.039	0.030	030516.5
*J*08595840−3828491	0.089	0.076	000116.0
*J*09081014−2819103	0.106	0.098	000405.8
*J*09322353+1146033	0.037	0.028	030516.6
*J*10345603−0020334	0.089	0.061	040507.8
*J*10351922−0237477	0.103	0.078	040510.8
*J*10453865−0441563	0.070	0.051	040507.8
*J*10484056−0157319	0.092	0.074	040510.8
*J*10484663+0839579	0.096	0.072	040507.9
*J*10505517+0429583	0.052	0.042	040510.8
*J*10523610−0012060	0.051	0.041	040510.9
*J*10524541+0206444	0.054	0.040	040510.9
*J*10560146+0611076	0.094	0.068	040507.9
*J*11064405+1744146	0.091	0.064	040507.9
*J*11085645+2015280	0.097	0.069	040507.9
*J*11103678+1118057	0.097	0.070	040507.9
*J*11151222+2305439	0.096	0.068	040507.9
*J*11353071+3452042	0.063	0.048	040510.9
*J*11392617+2743564	0.039	0.027	030517.7
*J*11460103+3255584	0.086	0.068	040511.0
*J*11543774+3708068	0.106	0.082	040511.0
*J*12160755+4039367	0.047	0.032	040511.8
*J*12194870+4859028	0.049	0.035	040511.8
*J*13120152+5622487	0.057	0.042	040508.8
*J*13122380+0051472	0.058	0.044	030519.0
*J*13151180+4215593	0.051	0.037	040508.8
*J*13330290−2317496	0.059	0.042	040507.9

Table 2. (Continued.)

name	RMS($v=1$) (K)	RMS($v=2$) (K)	Obsdate (yymmdd.d)
J14165935−1626201	0.080	0.058	040512.0
J14572697+0516034	0.047	0.034	040508.9
J14573501+6555572	0.063	0.046	040508.9
J15132577−1543595	0.074	0.061	050524.9
J15303981+4651311	0.058	0.041	040511.9
J15352130−2356492	0.068	0.054	050524.9
J15553694−2908555	0.095	0.076	040422.0
J16062376−3753547	0.155	0.122	040422.1
J16075796−2040087	0.043	0.032	040508.0
J16080176−3157131	0.099	0.079	040421.1
J16141835−3529559	0.069	0.086	040423.1
J16381308−2834098	0.095	0.071	040515.0
J16432728−1412001	0.059	0.050	040330.1
J16462440−2609490	0.079	0.095	040518.0
J16465797+7931489	0.041	0.030	040511.9
J17040479−1128350	0.080	0.069	040330.3
J17050065−2712574	0.064	0.052	050215.2
J17055212−2550378	0.082	0.062	050213.2
J17280279−3039095	0.133	0.100	040512.0
J17310332−2633475	0.070	0.053	050524.0
J17385962−2140226	0.057	0.077	040226.2
J18004498−1700346	0.084	0.068	040419.2
J18014609−2651329	0.083	0.062	040508.1
J18035617−1523263	0.118	0.096	050529.1
J18111163−2630028	0.084	0.067	040225.4
J18131385−1028218	0.119	0.096	040419.2
J18183077−2228418	0.107	0.079	050529.0
J18273952−0349520	0.162	0.132	040420.1
J18300605−1801423	0.093	0.092	060419.2
J18325074−1702485	0.068	0.051	040225.4
J18364067+0008011	0.131	0.106	040516.0
J18470154−0228028	0.084	0.064	040517.1
J18492153−0944574	0.129	0.124	060411.2
J18492433+0835397	0.129	0.107	040516.0
J18495464+0930071	0.146	0.119	040420.1
J18530277+0916373	0.086	0.089	060411.3
J18550975+0956101	0.093	0.096	060316.3
J18575369−0556101	0.075	0.064	060421.2
J18585052−0259278	0.156	0.112	050529.1
J19135861+0007319	0.062	0.048	040420.1
J19150117+0348427	0.093	0.074	040420.1
J21471812+2532560	0.065	0.049	040509.3
J21552697+2342144	0.077	0.056	040509.3
J21594957+2356270	0.079	0.059	040509.3
J22013668+6259263	0.072	0.054	040509.3
J22063830+2458144	0.081	0.063	040509.3
J22242842+1453433	0.086	0.067	040509.4
J23164760−2723338	0.046	0.034	040508.3
J23505380−3517479	0.159	0.120	040508.4

Table 3. Infrared properties of the observed sources

2MASS name	K (mag)	$J-H$ (mag)	$H-K$ (mag)	Bflag	MSX6C name	Δr_M ($''$)	F_C (Jy)	C_{AC}	C_{CE}	IRAS name	Δr_I ($''$)
J01015839+5759482	4.123	0.864	0.448	111	(124.332−04.846)		4.3†		−0.228†	00589+5743	5.1
J02005614+0945356	7.170	1.741	1.355	111	(149.845−49.446)		2.3†		−0.50†	01582+0931	1.4
J02151393+5613030	6.014	1.747	1.111	111	(134.439−04.771)		7.4†		−0.040†	02117+5559	2.5
J02160009−2031108	2.613	0.864	0.502	111	(198.593−69.596)		26.7†		−0.20†	02136−2045	7.1
J02300585+4007038	11.701	3.039	2.745	11	(142.651−18.946)		1.0†		−0.16†	02269+3953	0.6
J02311288+6340198	6.272	2.452	1.896	111	G133.7260+02.9110	1.5	6.13	−0.069	−0.346	02272+6327	3.1
J03055291+5420538	4.950	1.343	0.773	111	G141.7917−03.5248	1.3	7.60	−0.003	−0.099	03022+5409	5.7
J03133515+5948036	6.217	2.739	2.119	111	G139.9388+01.7086	1.1	12.25	0.003	−0.198	03096+5936	5.0
J03230583+5652435	4.778	2.206	1.556	111	G142.5510−00.1002	2.0	20.72	−0.041	−0.352	03192+5642	1.4
J03275901+6044553	5.240	2.935	2.196	111	(140.930+03.470)		70.4†		−0.275†	03238+6034	1.3
J03404991+4941534	9.057	2.547	2.307	111	G148.8464−04.4554	2.5	3.73	0.170	0.094	03371+4932	1.3
J03482812+1657032	11.097	1.195	0.806	111	(172.347−28.475)						
J03552337+1133437	11.526	1.520	1.004	111	(178.183−30.959)						
J03563582+5720279	4.389	1.189	0.715	111	(145.924+02.982)		7.1†		−0.205†	03525+5711	2.0
J03591178+4413103	7.161	3.322	2.528	111	(154.754−06.747)		36.3†		−0.087†	03557+4404	2.0
J03595596+0919044	10.114	1.528	1.115	111	(181.024−31.584)						
J04432934+3432189	4.816	1.218	0.666	111	(167.732−07.460)		3.4†		−0.229†	04402+3426	3.2
J04501343+3007449	5.218	1.104	0.636	111	(172.080−09.179)		5.9†		−0.118†	04470+3002	3.6
J05233987+3230157	4.840	1.620	0.931	111	G174.4448−02.0316	1.0	14.74	0.082	−0.018	05204+3227	6.8
J05301817+2022024	4.728	1.060	0.576	111	(185.423−07.501)		5.2†		−0.172†	05273+2019	5.5
J05434967+3242061	5.672	3.050	2.545	111	G176.5876+01.6391	1.2	286.90	0.039	−0.288	05405+3240	1.1
J05475868−3305109	6.152	0.935	0.656	111	(238.258−26.921)		2.0†		−0.06†	05461−3306	2.4
J05481570+2001593	5.896	2.477	1.889	111	(187.936−04.093)		15.7†		−0.213†	05452+2001	0.3
J05514643+3522189	7.529	2.285	2.019	111	(175.145+04.425)		8.0†		−0.288†	05484+3521	2.1
J06092550−0938492	7.651	1.107	1.361	111	(216.897−13.672)		9.7†		0.039†	06070−0938	6.1
J06181637−1702347	7.986	0.445	0.611	111	(224.751−14.854)		3.5†		−0.152†	06160−1701	3.3
J06195821−1038146	3.655	1.432	1.490	111	(218.968−11.765)		422.0†		0.034†	06176−1036	11.9
J06204380−0433270	‡				(213.512−8.902)		7.6†		0.155†	06182−0432	
J06215148−0350416	5.569	1.769	1.400	111	(212.997−08.330)		86.1†		−0.148†	06193−0349	3.2
J06243845−1753432	3.427	1.270	0.366	111	(226.200−13.823)		7.0†		−0.183†	06224−1751	7.0
J06265390−1015349	7.633	1.182	1.204	111	(219.379−10.067)		3.3†		0.198†	06245−1013	7.5
J06342805−0503427	5.704	1.270	1.235	111	(215.521−06.074)		51.2†		0.101†	06319−0501	28.7
J06353168−0109256	3.685	1.244	0.812	111	G212.1476−04.0680	3.1	18.80	0.023	−0.022	06329−0106	3.3
J06370162−0127018	11.289	1.784	3.641	20	G212.5806−03.8674	0.5	14.93	0.175	−0.070	06344−0124	3.5
J06413391−0806289	6.876	2.407	2.019	111	(219.054−05.869)		13.7†		−0.168†	06391−0803	11.8
J06421530−0939442	2.847	1.272	0.702	111	(220.529−06.412)		31.5†		−0.170†	06398−0936	4.6
J06425082−0141061	7.017	3.604	2.477	111	G213.4533−02.6799	2.3	13.94	0.135	0.067	06403−0138	1.2
J06440823−1320089	6.012	1.226	0.732	111	(224.052−07.629)		2.8†		−0.100†	06418−1317	14.0
J06470984−0358461	4.324	1.149	0.578	111	G215.9898−02.7621	2.0	6.37	0.097	−0.119	06446−0355	1.1
J06472497+0813588	5.536	2.216	1.850	111	G205.1419+02.8568	2.1	26.50	−0.063	−0.329	06447+0817	11.1
J06474716+1636326	5.823	1.854	1.546	111	(197.674+06.705)		5.8†		−0.298†	06448+1639	2.8
J06505251−0004235	2.334	1.141	0.416	111	G212.9327−00.1585	1.1	15.29	−0.051	−0.114	06483−0000	7.5
J06513922−2123303	6.834	1.930	1.560	111	(232.174−09.528)		3.1†		−0.52†	06495−2119	3.0
J06522047−0328407	4.260	0.861	0.472	111	(216.131−01.385)		2.5†		−0.123†	06498−0324	5.8
J06530149−0453501	0.295	2.884	3.670	11	G217.4725−01.8788	0.2	25.35	0.041	−0.191	06505−0450	3.2
J06551745−1647526	4.106	1.018	0.586	111	(228.381−06.745)		3.6†		−0.159†	06530−1643	0.8
J06552346−2122258	6.576	1.837	1.454	111	(232.539−08.736)		3.4†		−0.51†	06532−2118	3.0
J07065685−1109395	10.172	3.384	3.383	11	G224.6212−01.6745	1.5	5.42	0.089	−0.244	07045−1104	1.0
J07072736−2538440	4.275	0.834	0.608	111	(237.646−08.124)		4.7†		−0.188†	07054−2533	0.6
J07074938−1044059	3.651	1.650	1.240	111	G224.3419−01.2881	1.5	94.56	−0.029	−0.107	07054−1039	4.6
J07112217−0129391	3.881	0.983	0.301	111	(216.540+03.749)		9.2†		−0.198†	07088−0124	4.4
J07122348−0124521	4.615	0.908	0.423	111	G216.5881+04.0135	6.9	2.83	0.126	—	07098−0119	4.9
J07132317−2752580	8.030	2.138	1.955	111	(240.264−07.934)		17.5†		0.182†	07113−2747	2.0

Table 3. (Continued.)

2MASS name	K (mag)	$J-H$ (mag)	$H-K$ (mag)	Bflag	MSX6C name	Δr_M ($''$)	F_C (Jy)	C_{AC}	C_{CE}	IRAS name	Δr_I ($''$)
J07132320−0718336	6.724	1.083	0.685	111	G221.9378+01.5128	0.6	2.64	−0.044	−0.100	07109−0713	3.3
J07143791−2513019	6.335	1.566	1.265	111	(237.992−06.484)		1.6†		−0.75†	07125−2507	19.1
J07172817−2417135	5.309	1.786	1.555	111	(237.456−05.486)		35.3†		−0.128†	07153−2411	5.5
J07184575−2123318	9.897	3.063	2.556	111	G235.0167−03.8847	2.1	3.13	0.065	−0.192†	07166−2117	4.8
J07201954−1320137	3.534	1.791	1.190	111	G228.0663+00.2106	0.8	24.51	0.083	0.046	07180−1314	1.9
J07221634−1852159	6.258	1.871	1.413	111	G233.1713−01.9786	1.8	12.30	0.056	−0.022	07200−1846	5.1
J07243912−0437541	5.818	1.226	0.768	111	(220.869+05.238)		5.4†		0.093†	07221−0431	17.3
J07251926−1121214	7.055	2.729	2.208	111	(226.894+02.221)		5.1†		−0.14†	07229−1115	11.9
J07291120−2610322	4.088	0.908	0.435	111	(240.373−04.024)		3.4†		−0.111†	07271−2604	7.1
J07321227−2147136	3.429	1.065	0.505	111	G236.8450−01.3185	1.3	13.56	0.047	−0.132	07300−2140	1.8
J07364088−1018431	3.797	0.868	0.450	111	(227.310+05.170)		5.4†		−0.184†	07343−1011	2.5
J07394181−2834172	5.634	1.163	0.869	111	G243.6025−03.1359	1.0	21.64	0.051	0.049	07376−2827	3.1
J07445699−1541500	3.115	0.896	0.349	111	(233.011+04.294)		19.0†		−0.145†	07426−1534	1.8
J07454092−1854291	11.511	2.587	3.229	11	G235.8880+02.8468	1.9	12.06	0.108	−0.114	07434−1847	1.8
J07454503−3619503	—	—	—	—	(251.009−05.844)	–	10.8†		−0.145†	07439−3612	6.6
J07463415−3218165	2.020	1.046	0.595	111	G247.5863−03.6967	1.7	136.20	0.064	−0.167	07446−3210A	5.7
J07493363−2546454	6.930	0.883	0.439	111	G242.2774+00.1587	2.2	2.22	−0.053	0.015	07474−2539	6.8
J07493726−3820439	9.183	2.777	2.448	111	(253.151−06.176)		2.5†		−0.18†	07478−3813	1.8
J07494088−3933293	3.477	1.029	0.717	111	(254.215−06.770)		26.8†		−0.136†	07479−3925	3.7
J07495786−3654299	6.898	1.024	0.477	111	(251.935−05.398)		4.7†		0.038†	07481−3646	0.8
J07514440−3519526	4.816	1.266	0.832	111	G250.7506−04.2919	2.8	9.38	−0.048	−0.242	07498−3512	6.6
J07521749−0329044	4.231	0.815	0.546	111	(223.145+11.853)		5.1†		−0.15†	07497−0321	15.1
J07531683−1129311	5.768	1.148	0.716	111	(230.357+08.143)		12.7†		−0.166†	07509−1121	0.9
J07554019−2838544	2.581	0.976	0.475	111	G245.4381−00.1478	3.0	84.55	0.064	−0.018	07536−2830	3.2
J07585240−0122349	3.204	1.142	0.413	111	(222.051+14.305)		9.3†		−0.19†	07563−0114	0.2
J08003235−3559477	8.045	2.097	1.508	111	G252.2454−03.1055	1.1	1.64	0.047	0.045	07586−3551	1.6
J08004940−3655221	5.006	1.315	0.943	111	G253.0650−03.5430	0.7	6.98	0.035	−0.243	07589−3647	7.5
J08020499−3811522	4.668	1.135	0.664	111	G254.2826−04.0008	3.8	32.15	0.079	0.095	08002−3803	7.1
J08031918−3138009	4.441	0.831	0.645	111	G248.8462−00.3074	0.4	4.94	0.013	−0.206	08013−3129	2.6
J08043072−0307483	5.252	1.735	1.225	111	(224.340+14.695)		6.7†		−0.192†	08019−0259	2.1
J08102688−3914152	10.157	2.409	3.266	111	G256.0388−03.1799	1.8	29.12	0.099	−0.149	08086−3905	3.0
J08104779−3520442	4.242	1.666	1.063	111	G252.8129−00.9980	1.7	23.79	0.118	0.020	08089−3511	3.0
J08105244−3515260	4.887	1.244	0.626	111	G252.7476−00.9362	0.8	12.36	−0.043	−0.020	08089−3506	3.0
J08121082−2343485	4.098	0.810	0.577	111	(243.237+05.603)		10.8†		−0.118†	08100−2334	6.0
J08141230−4142291	3.782	1.416	1.199	111	G258.5012−03.9346	2.5	129.20	0.133	−0.066	08124−4133	2.5
J08144298−3233047	8.439	2.777	2.173	111	G250.9283+01.2198	0.4	9.41	0.110	0.048	08127−3223	3.4
J08160288−3536539	9.296	2.632	1.969	111	G253.6280−00.2553	1.1	1.62	0.087	0.153	08141−3527	2.6
J08191830−2144143	13.441	0.225	3.499	1	(242.465+08.069)		120.0†		0.031†	08171−2134	7.1
J08200755−2616323	4.526	0.863	0.152	111	(246.369+05.699)		3.6†		−0.160†	08180−2607	1.1
J08214679−1346410	12.316	2.564	3.665	11	(236.008+12.907)		3.2†		−0.18†	08194−1337	0.4
J08221114−2537546	1.284	0.928	0.336	111	(246.094+06.444)		44.8†		−0.183†	08200−2528	0.9
J08255320−3333507	3.417	1.179	0.282	111	G253.0888+02.5758	1.9	15.14	0.031	−0.141	08239−3323	1.4
J08293488−3836214	7.915	0.146	0.364	111	G257.6236+00.2459	1.1	1.73	0.035	0.181	08277−3826	4.1
J08333853−3707051	7.026	2.089	1.318	111	G256.8978+01.7722	0.3	1.65	−0.007	0.062	08317−3656	4.2
J08362321−4057172	9.263	3.536	3.154	111	G260.2896−00.0992	0.4	5.38	0.071	−0.234	08345−4046	17.4
J08392931−4013441	8.818	0.993	0.691	111	G260.0693+00.8090	1.5	1.79	0.217	0.100	08376−4003	8.9
J08400691−0813472	3.839	0.976	0.794	111	(233.675+19.690)		12.8†		−0.20†	08376−0803	3.0
J08451851+1420341	12.379	1.092	0.969	111	(212.266+31.598)						
J08595840−3828491	7.108	1.826	1.215	111	(261.218+04.982)		4.1†		−0.052†	08580−3817	1.2
J09045184−2810357	4.677	1.292	0.962		(253.986+12.477)		12.8†		−0.058†	09027−2758	
J09081014−2819103	6.949	1.070	1.111		(254.583+12.936)		3.8†		−0.174†	09060−2807	7.8
J09220626−2934129	4.231	1.309	1.125	111	(257.642+14.358)		33.5†		−0.181†	09199−2921	3.7
J09322353+1146033	9.589	1.167	1.184	111	(221.069+40.982)		2.0†		0.17†	09296+1159	4.1
J10255751−0730506	3.364	1.061	0.593	111	G252.1851+40.6053	0.8	12.33	−0.084	−0.216		

Table 3. (Continued.)

2MASS name	K (mag)	$J-H$ (mag)	$H-K$ (mag)	Bflag	MSX6C name	Δr_M ($''$)	F_C (Jy)	C_{AC}	C_{CE}	IRAS name	Δr_I ($''$)
J10345603−0020334	3.699	1.045	0.409	111	G247.2370+47.2220	3.5	2.95	−0.208	−0.237		
J10351922−0237477	3.616	0.918	0.312	111	G249.7395+45.7157	3.0	1.81	−0.191	—		
J10453865−0441563	3.897	0.828	0.423	111	G254.4673+46.0008	0.8	1.98	−0.099	—	10431−0426	8.9
J10484056−0157319	1.749	0.756	0.233	111	G252.5530+48.5308	3.7	6.18	−0.327	−0.506		
J10484663+0839579	1.706	0.997	0.397	111	G239.6370+55.6395	1.1	26.27	−0.014	−0.200		
J10505517+0429583	4.054	0.814	0.489	111	G245.8008+53.4319	2.1	0.96	−0.217	—		
J10523610−0012060	2.730	0.812	0.271	111	G251.7823+50.4781	3.7	2.36	−0.354	—	10500+0003	3.5
J10524541+0206444	2.926	1.015	0.178	111	G249.2132+52.1467	1.0	2.60	−0.293	—		
J10533744+1342544	1.800	0.893	0.485	111	G233.0233+59.4269	3.3	34.06	−0.014	−0.322		
J10560146+0611076	−0.762	0.883	0.313	111	G245.0506+55.4966	2.5	78.61	−0.255	−0.441		
J11064405+1744146	2.579	0.808	0.196	111	G228.6984+64.1142	1.7	3.08	−0.301	−0.525		
J11085645+2015280	1.796	0.969	0.265	111	G223.7528+65.6028	1.5	5.85	−0.245	−0.386		
J11103678+1118057	1.581	0.875	0.296	111	G241.7906+61.5209	1.3	10.27	−0.259	−0.499		
J11151222+2305439	−0.074	0.851	0.229	111	G218.0959+67.8810	1.5	31.83	−0.282	−0.493		
J11353071+3452042	−0.222	0.903	0.362	111	G182.7804+72.0228	3.0	145.40	0.066	−0.276		
J11392617+2743564	13.036	1.971	2.047	111	(206.611+74.026)						
J11414026+3828293	5.078	0.696	0.516	111	G170.6827+71.5176	2.2	2.78	−0.134	−0.345	11390+3845	9.0
J11460103+3255584	3.143	1.018	0.499	111	G186.6680+74.7197	1.7	2.02	−0.322	−0.215		
J11543774+3708068	2.700	0.851	0.474	111	G169.5450+74.3872	0.8	5.99	−0.125	−0.185		
J12160755+4039367	1.644	0.896	0.065	111	G148.9833+74.6315	6.2	6.59	−0.371	−0.387		
J12194870+4859028	1.042	0.803	0.235	111	G136.4621+67.3044	2.4	10.53	−0.333	−0.480	12173+4915	8.2
J13120152+5622487	1.853	0.982	0.592	111	G117.1393+60.5156	1.6	15.13	−0.122	−0.258	13099+5638	3.8
J13122380+0051472	12.650	1.939	2.360	11	(314.640+63.257)						
J13151180+4215593	2.953	0.954	0.330	111	G106.6951+74.1043	0.5	4.40	−0.193	−0.403	13129+4231	3.6
J13330290−2317496	13.442	1.857	1.100	111	(315.181+38.583)						
J14165935−1626201	0.568	0.961	0.385	111	(330.886+41.742)			63.5†	−0.27†	14142−1612	0.5
J14280928−3300034	5.830	1.398	1.452	111	(325.327+25.630)			34.5†	−0.18†	14251−3246	5.6
J14572697+0516034	11.438	1.566	1.238	111	(002.520+52.890)						
J14573501+6555572	−0.957	0.883	0.183	111	G104.8717+46.5257	1.2	85.32	−0.267	−0.468	14567+6607	3.0
J15132577−1543595	8.573	1.064	1.065	111	(345.966+35.014)		6.1†		0.16†	15106−1532	4.3
J15303981+4651311	3.113	0.963	0.486	111	G076.0462+53.1519	1.4	2.36	—	—	15290+4701	1.3
J15331652−1519350	2.580	0.930	0.549	111	(350.613+32.178)		15.9†		−0.44†	15304−1509	0.4
J15332161−2711031	2.116	0.929	0.590	111	(341.854+23.195)		34.3†		−0.42†	15303−2700	3.2
J15352130−2356492	4.553	0.753	0.518	111	(344.498+25.403)		5.6†		−0.34†	15323−2346	6.5
J15463127−2107395	3.831	0.841	0.501	111	(348.712+25.792)		6.8†		−0.39†	15436−2058	1.3
J15553694−2908555	3.113	0.991	0.309	111	(344.461+18.506)		5.4†		−0.29†	15525−2900	8.4
J16015727−3846475	3.347	0.902	0.985	111	(338.785+10.485)		18.9†		−0.27†	15586−3838	1.5
J16055729−2747309	5.320	1.102	0.642	111	(347.178+17.924)		6.1†		−0.13†	16028−2739	2.3
J16062376−3753547	2.969	1.250	0.399	111	(340.044+10.548)		8.0†		−0.28†	16030−3745	8.5
J16075796−2040087	7.808	1.756	1.497	111	(352.951+22.576)		1.5†		0.18†	16050−2032	2.9
J16080176−3157131	4.659	0.900	0.630	111	(344.484+14.632)		8.0†		−0.29†	16048−3149	4.2
J16141835−3529559	4.322	1.350	0.884	111	(342.900+11.185)		9.9†		−0.24†	16110−3522	1.8
J16203527−3209370	5.690	1.492	1.102	111	(346.265+12.601)		12.8†		−0.13†	16173−3202	0.5
J16324854−2623062	3.649	1.087	0.676	111	(352.502+14.521)		16.1†		−0.36†	16297−2616	4.7
J16381308−2834098	3.029	1.204	0.553	111	(351.602+12.188)		10.1†		−0.42†	16350−2828	7.4
J16395065−2406083	3.691	1.486	0.828	111	(355.366+14.776)		10.1†		−0.39†	16368−2400	1.8
J16432728−1412001	8.645	2.967	2.566	111	(004.102+20.200)		25.7†		−0.28†	16406−1406	0.8
J16462440−2609490	7.217	1.429	1.063	111	(354.685+12.323)		3.4†		−0.07†	16433−2604	8.2
J16465797+7931489	13.927	1.636	1.276	111	(112.345+32.139)						
J16521293−1257016	1.973	1.187	0.787	111	(006.502+19.204)		84.2†		−0.28†	16494−1252	1.4
J16543110−0733376	3.008	1.371	0.512	111	(011.601+21.766)		11.1†		−0.28†	16518−0728	1.1
J17001324−1037003	3.607	1.418	1.023	111	(009.710+18.906)		89.6†		−0.24†	16574−1032	1.6
J17030696−2033255	2.327	1.243	0.648	111	(001.632+12.665)		45.5†		−0.16†	17001−2029	5.3
J17040479−1128350	4.483	0.877	0.540	111	(009.508+17.642)		6.3†		−0.22†	17013−1124	4.4

Table 3. (Continued.)

2MASS name	K (mag)	$J-H$ (mag)	$H-K$ (mag)	Bflag	MSX6C name	Δr_M ($''$)	F_C (Jy)	C_{AC}	C_{CE}	IRAS name	Δr_I ($''$)
J17050065−2712574	4.376	0.971	0.733	111	(356.418+08.391)		7.2†		−0.37†	17018−2708	3.5
J17055212−2550378	6.710	1.511	1.147	111	(357.652+09.049)		11.8†		−0.10†	17027−2546	4.3
J17061081−1028590	2.485	1.201	0.536	111	(010.677+17.757)		22.6†		−0.22†	17034−1024	3.9
J17121537−1637006	5.387	1.367	0.896	111	(006.219+13.136)		10.3†		−0.13†	17093−1633	7.8
J17272810−3047542	4.554	1.450	0.842	111	G356.3125+02.3153	0.5	6.32	0.059	−0.294	17242−3045	4.7
J17280279−3039095	7.553	2.787	1.636	200	G356.5031+02.2926	3.7	4.84	0.069	0.018	17248−3036	23.2
J17310332−2633475	10.006	2.772	3.133	11	G000.2871+03.9915	1.5	7.14	0.099	0.036	17279−2631	2.1
J17334246−2633545	6.692	2.697	1.820	111	G000.6088+03.4930	2.9	7.45	0.050	−0.160	17305−2631	11.4
J17335931−2659216	7.963	3.603	2.344	200	G000.2854+03.2107	2.7	7.70	0.084	−0.034	17308−2657	1.8
J17365144−2516262	5.780	2.156	1.273	111	G002.0815+03.5905	3.5	11.77	0.100	−0.054	17337−2514	1.9
J17365757−2418066	8.403	2.066	2.243	11	G002.9167+04.0899	0.4	8.56	0.150	−0.086	17339−2416	4.8
J17373815−2557269	4.366	1.513	0.827	111	G001.5967+03.0773	4.3	7.48	0.043	−0.343	17345−2555	2.4
J17385962−2140226	2.366	1.064	0.434	111	(005.401+05.089)		13.1†		−0.28†	17359−2138	6.0
J17394268−2134239	6.476	2.737	1.928	111	G005.5741+04.9999	0.2	13.10	0.023	−0.057	17367−2132	8.6
J17415458−2047055	2.787	1.629	0.912	111	G006.5177+04.9771	1.3	69.95	0.036	−0.014	17389−2045	13.6
J17431835−2109031	5.984	1.645	1.181	111	G006.3750+04.5082	1.0	7.52	0.010	−0.097	17403−2107	15.4
J17441045−2215239	5.583	2.269	1.458	111	G005.5338+03.7601	1.0	13.29	0.077	−0.053	17411−2214	22.4
J17454035−2223291	6.192	2.127	1.764	111	G005.5987+03.3939	1.5	20.23	0.078	−0.042	17426−2222	2.6
J17472779−2058089	4.126	1.250	0.874	111	G007.0341+03.7721	2.9	16.45	−0.015	−0.287	17444−2057	22.1
J17532342−1902545	5.360	1.650	1.148	111	G009.4014+03.5536	0.5	7.41	0.044	−0.075	17504−1902	2.8
J17551128−1852359	4.132	1.521	0.836	111	G009.7645+03.2730	0.2	7.22	0.032	−0.221	17522−1852	6.6
J17555714−1531531	4.261	1.194	0.783	111	(012.760+04.789)		14.6†		−0.27†	17530−1531	2.9
J17572314−1802456	3.546	1.198	0.733	111	G010.7465+03.2368	3.4	11.31	0.003	−0.179	17544−1802	4.3
J17573605−1825517	6.836	2.321	1.496	11	G010.4376+03.0008	4.3	8.44	0.070	−0.131	17546−1825	6.8
J17593665−1735346	9.072	1.206	2.331	11	G011.4038+03.0029	2.1	7.87	0.056	0.006	17566−1735	14.0
J18001195−2947267	5.376	1.850	1.247	111	G000.8772−03.1703	1.0	10.12	0.042	0.085	17570−2947	2.5
J18004498−1700346	3.827	1.266	0.838	111	G012.0459+03.0552	2.1	31.42	−0.052	−0.084	17578−1700	2.3
J18014609−2651329	6.806	2.020	1.305	111	G003.5997−02.0222	1.5	5.21	0.061	0.019	17586−2651	7.6
J18035617−1523263	5.065	1.251	0.888	111	G013.8342+03.1845	2.3	7.14	−0.031	−0.155	18010−1523	3.0
J18083501−2609029	7.711	2.999	1.979	111	G004.9634−03.0070	1.1	7.50	0.047	0.001	18054−2609	3.1
J18085198−2616210	2.540	2.019	0.935	111	G004.8872−03.1215	1.8	80.42	−0.006	−0.201	18057−2616	4.6
J18100465−2559418	4.709	1.206	0.742	111	G005.2620−03.2259	0.9	8.85	−0.018	−0.168	18069−2600	4.0
J18111148−2705565	3.231	1.325	0.622	111	G004.4104−03.9736	1.3	8.63	−0.017	−0.377	18080−2706	8.4
J18111163−2630028	2.442	1.676	0.595	111	G004.9375−03.6882	1.4	19.55	0.061	−0.275		
J18121417−2243588	6.173	1.679	1.037	111	G008.3630−02.0909	0.6	1.32	0.031	—	18092−2244	1.3
J18125638−2434279	4.023	1.427	0.994	111	G006.8215−03.1136	1.3	24.58	−0.009	−0.141	18098−2435	1.8
J18130340−2451495	2.778	1.361	0.684	111	G006.5792−03.2749	1.2	23.30	0.049	−0.306	18099−2452	5.2
J18131385−1028218	2.611	1.359	0.713	111	G019.2438+03.5743	0.6	13.11	−0.030	−0.151	18104−1029	1.8
J18135525−1047054	4.318	1.564	0.933	111	G019.0495+03.2766	0.4	21.94	0.011	−0.169	18111−1048	1.0
J18144245−2355098	4.680	1.066	0.701	111	G007.5906−03.1560	1.9	7.02	−0.031	−0.240	18116−2356	3.7
J18182505−0825596	5.086	1.507	1.002	111	G021.6502+03.4141	4.1	7.084	0.072	−0.193	18156−0827	9.0
J18183077−2228418	6.296	1.781	1.171	111	G009.2762−03.2445	0.4	8.07	0.032	−0.136	18154−2229	2.9
J18183625−0812320	6.438	2.459	1.600	111	G021.8707+03.4771	2.7	13.16	0.098	−0.030	18158−0813	5.1
J18192924−2302044	4.488	1.082	0.790	111	G008.8901−03.7045	1.0	12.09	−0.033	−0.228	18164−2303	1.2
J18194627−2352057	5.798	1.332	1.200	111	G008.1828−04.1522	1.8	12.21	0.047	−0.107	18166−2353	35.7
J18202016−2303504	5.534	1.978	1.515	111	G008.9558−03.8905	0.8	48.47	0.042	−0.103	18172−2305	12.5
J18223070−2041121	7.284	2.980	2.027	111	G011.2983−03.2262	2.4	7.432	0.126	0.001	18195−2042	8.1
J18231258−2100114	3.665	1.283	0.648	111	G011.0941−03.5183	3.8	23.74	−0.040	−0.198	18202−2101	4.6
J18252822−2205007	3.508	1.378	0.705	111	G010.3785−04.4838	2.0	14.38	0.001	−0.124	18224−2206	5.5
J18253701−2153267	5.235	1.451	1.213	111	G010.5657−04.4249	1.9	22.38	−0.009	−0.123	18226−2155	6.0
J18263203−0443370	5.962	2.412	1.813	111	G025.8761+03.3593	3.9	15.60	0.041	−0.020	18238−0445	4.4
J18264589−1925293	5.731	1.691	1.217	111	G012.8823−03.5242	2.4	7.677	−0.011	−0.059	18238−1927	6.1
J18270303−2014544	4.744	1.587	0.958	111	G012.1821−03.9649	5.4	8.020	−0.056	−0.168	18240−2016	3.8
J18272475−0357552	4.916	2.219	1.343	111	G026.6530+03.5176	4.9	19.48	0.030	−0.102	18247−0359	9.8

Table 3. (Continued.)

2MASS name	K (mag)	$J-H$ (mag)	$H-K$ (mag)	Bflag	MSX6C name	Δr_M ($''$)	F_C (Jy)	C_{AC}	C_{CE}	IRAS name	Δr_I ($''$)
J18272645−0422462	5.385	1.791	1.227	111	G026.2894+03.3194	5.1	8.601	−0.006	−0.159	18247−0424	4.3
J18273952−0349520	3.041	1.740	1.346	111	G026.8015+03.5262	0.4	124.70	−0.054	−0.038	18250−0351	11.7
J18281254−0417486	4.246	1.634	1.033	111	G026.4509+03.1885	3.2	7.349	−0.056	−0.166	18255−0419	26.2
J18300605−1801423	7.813	2.318	1.727	111	G014.4884−03.5803	1.0	7.672	0.039	−0.181	18271−1803	6.2
J18325074−1702485	5.310	1.661	1.254	111	G015.6638−03.7108	2.2	27.75	0.362	0.286	18299−1705	3.5
J18343099−0025046	5.477	2.503	1.403	111	G030.6269+03.5729	2.7	12.22	0.083	−0.153	18319−0027	9.3
J18350137−1545026	4.390	1.561	1.026	111	G017.0584−03.5821	3.6	17.55	−0.038	−0.105	18321−1547	10.8
J18364067+0008011	6.032	2.618	1.667	111	G031.3652+03.3445	4.8	9.94	0.071	−0.028	18341+0005	4.5
J18364919−1351561	3.600	1.196	0.588	111	G018.9358−03.1069	0.5	10.50	−0.082	−0.268	18339−1354	8.5
J18380663+0229591	5.501	1.735	1.079	111	G033.6401+04.1048	4.1	8.951	0.033	−0.087	18355+0227	16.5
J18393585−1231005	4.323	1.642	0.940	111	G020.4463−03.0929	1.4	21.92	0.026	−0.112	18367−1233	3.1
J18425242−1210401	4.826	1.992	1.381	111	G021.1129−03.6518	2.9	21.59	0.056	−0.168	18400−1213	9.7
J18451857−1010551	4.237	1.580	0.847	111	G023.1669−03.2781	0.3	17.79	0.058	−0.110	18425−1014	1.0
J18454730+0527211	4.496	1.395	0.805	111	(037.152+03.738)		14.37		−0.172	18433+0524	4.4
J18455342−1203361	5.906	2.616	1.909	111	G021.5527−04.2557	2.8	13.72	0.030	−0.077	18430−1206	3.1
J18470154−0228028	13.569	0.957	0.534	111	(030.233−00.144)		14.4†		−0.17†	18443−0231	50.2
J18475335−0919102	4.028	2.060	1.413	111	G024.2258−03.4534	1.0	58.68	0.048	−0.137	18450−0922	51.5
J18475454−0821287	3.076	1.580	0.881	111	G025.0860−03.0226	2.3	55.21	0.011	−0.119	18451−0824	2.9
J18484390−1141297	3.444	1.458	0.800	111	G022.1971−04.7105	3.6	24.65	0.002	−0.222	18459−1144	3.7
J18492153−0944574	2.884	1.215	0.490	111	G024.0057−03.9713	0.4	7.542	−0.082	−0.336	18466−0948	7.4
J18492433+0835397	1.964	1.089	0.484	111	(040.365+04.356)		16.0†		−0.37†	18470+0832	2.3
J18495125−0939299	3.244	1.581	0.757	111	G024.1425−04.0390	0.2	16.70	0.043	−0.331	18471−0942	27.9
J18495464+0930071	6.953	2.877	2.716	111	G041.2340+04.6520	4.6	208.60	0.060	−0.272	18475+0926	1.8
J18500474+0559286	5.245	2.466	1.713	111	G038.1146+03.0292	0.5	20.15	0.118	−0.043	18476+0555	4.9
J18503766+0409088	9.973	2.659	3.454	111	G036.5373+02.0723	3.3	5.04	0.146	0.121	18481+0405	6.5
J18530277+0916373	4.961	1.818	1.308	111	G041.3824+03.8617	1.7	7.308	0.092	−0.012	18506+0912	4.8
J18532358−2620122	3.235	1.103	0.511	111	(009.341−12.070)		11.3†		−0.07†	18502−2623	4.5
J18541840−0648564	3.987	1.152	0.826	111	G027.1835−03.7372	2.0	18.83	−0.016	−0.301	18516−0652	3.2
J18542609+1018031	4.968	1.483	1.035	111	G042.4531+04.0195	1.8	6.645	0.005	−0.035	18520+1014	7.8
J18550975+0956101	5.365	1.893	1.337	111	G042.2089+03.6940	2.1	8.881	−0.101	−0.437	18527+0952	2.3
J18551284+1041470	2.985	1.276	0.661	111	G042.8937+04.0266	1.3	12.81	−0.046	−0.233	18528+1037	5.7
J18575369−0556101	4.134	0.954	0.646	111	G028.3739−04.1339	1.6	8.642	0.019	−0.039	18552−0600	0.4
J18585052−0259278	6.587	3.561	2.442	111	G031.1112−03.0097	1.5	13.61	0.140	0.087	18562−0303	5.2
J18590806+1051001	4.654	1.777	1.118	111	G043.4681+03.2379	0.9	36.76	0.015	−0.121	18567+1046	8.5
J19012350−2726106	4.449	0.970	0.700	111	(009.055−14.146)		10.2†		−0.17†	18582−2730	1.7
J19012574−0529398	4.629	1.283	0.837	111	G029.1672−04.7190	1.0	21.16	0.000	−0.210	18587−0534	7.5
J19014986−1910383	5.180	2.230	1.445	111	(016.804−10.830)		25.6†		−0.06†	18588−1915	2.9
J19022521−2037492	5.086	1.153	0.808	111	(015.521−11.570)		5.8†		−0.24†	18594−2042	0.5
J19040549−0320389	3.126	1.548	0.598	111	G031.3916−04.3371	1.4	9.612	0.024	−0.388	19014−0325	1.0
J19061474+0002251	3.619	1.308	0.715	111	G034.6580−03.2758	1.5	25.27	−0.017	−0.193	19036−0002	2.2
J19085920−1510032	5.867	1.370	1.054	111	(021.237−10.662)		8.3†		−0.11†	19061−1514	4.2
J19123923−2341470	4.862	1.670	1.095	111	(013.644−14.986)		8.3†		−0.09†	19096−2346	2.1
J19135861+0007319	4.728	0.373	0.270	111	G035.6204−04.9552	2.4	25.27	0.705	1.340	19114+0002	1.8
J19150117+0348427	5.650	0.827	1.426	111	G039.0217−03.4912	1.8	26.48	0.033	−0.070	19125+0343	5.6
J19173939−1322488	4.712	1.078	0.821	111	(023.802−11.792)		9.2†		−0.20†	19148−1328	5.1
J19221604+0506593	3.276	1.383	0.690	111	G041.0209−04.4857	1.4	24.45	−0.038	−0.107	19198+0501	6.0
J19222258−1418050	5.598	1.886	1.400	111	(023.449−13.221)		8.8†		0.17†	19195−1423	3.9
J19235554−1302029	9.747	1.946	1.467	111	(024.791−13.023)		1.1†		0.26†	19211−1307	8.5
J19291840−1916199	4.220	0.839	0.570	111	(019.466−16.779)		11.9†		−0.19†	19263−1922	2.7
J19302125−1232535	5.905	1.288	0.889	111	(025.931−14.233)		4.2†		−0.25†	19275−1239	0.9
J19310440−1640135	5.054	1.405	1.086	111	(022.125−16.112)		24.7†		−0.11†	19281−1646	9.2
J19465644−0822022	5.685	2.032	1.633	111	(031.660−16.112)		29.8†		−0.02†	19442−0829	4.5
J21471812+2532560	2.912	1.097	0.519	111	G078.8031−21.1479	1.9	6.24	−0.140	−0.269		
J21552697+2342144	5.503	1.915	1.483	111	G078.9105−23.7599	1.3	7.47	−0.068	−0.651		

Table 3. (Continued.)

2MASS name	K (mag)	$J-H$ (mag)	$H-K$ (mag)	Bflag	MSX6C name	Δr_M ($''$)	F_C (Jy)	C_{AC}	C_{CE}	IRAS name	Δr_I ($''$)
J21582555+6343270	3.752	1.317	0.938	111	G105.1364+07.0029	1.7	11.56	0.057	−0.375	21570+6329	4.6
J21594957+2356270	−0.408	1.015	0.372	111	G079.8977−24.2547	1.1	66.58	−0.233	−0.474		
J22013668+6259263	4.605	1.012	0.551	111	G104.9712+06.2029	1.3	2.15	−0.064	−0.365	22001+6244	3.0
J22063830+2458144	2.089	0.985	0.419	111	G081.9246−24.4909	0.4	8.15	−0.178	−0.336	22043+2443	5.0
J22242842+1453433	4.067	0.408	0.590	111	G078.1196−34.8903	0.9	0.80	−0.280	—		
J23164760−2723338	11.462	3.529	2.475	111	G026.7412−68.9975	2.5	−0.64	—	—		
J23505380−3517479	3.183	0.997	0.391	111	G356.9034−74.7216	1.7	5.67	−0.062	−0.177		
J23584412−3926599	0.165	0.970	0.636	111	G341.2554−73.5111	1.3	289.00	0.052	−0.187		

† indicates IRAS 12 μm flux density in column F_C and
logrithmic ratio of IRAS 25 to 12 μm flux-densities in column C_{CE}.
‡ no 2MASS object, but the IRAS position is shown.

Table 4. Properties of the observed sources for dwarf galaxy member candidates.

2MASS name	Group	V_{GSR}^{SiO} (km s^{-1})	$\Lambda_\odot$ (deg)	$\beta_\odot$ (deg)	K (mag)	$H-K$ (mag)	A_K (mag)	$D^{\S}$ (kpc)	F_C (Jy)	IRAS name
*J*02005614+0945356	Sgr		109.1	−10.1	7.170	1.355	0.025	7	2.3	01582+0931
*J*02300585+4007038	Sgr		133.0	−32.0	11.701	2.745	0.021	20	1.0	02269+3953
*J*03482812+1657032	Sgr		135.6	−3.3	11.097	0.806	0.116	> 30		
*J*03552337+1133437	Sgr		134.6	2.2	11.526	1.004	0.088	> 30		
*J*03595596+0919044	Sgr		134.5	4.7	10.114	1.115	0.101	29		
*J*05475868−3305109	CMa	−56.0	138.3	54.2	6.152	0.656	0.012	7	2.0	05461−3306
*J*06513922−2123303	CMa		166.9	49.1	6.834	1.560	0.108	5	3.1	06495−2119
*J*06552346−2122258	CMa		168.2	49.3	6.576	1.454	0.119	5	3.4	06532−2118
*J*07143791−2513019	CMa		173.6	54.1	6.335	1.265	0.160	5	1.6	07125−2507
*J*07251926−1121214	CMa		181.0	40.9	7.055	2.208	0.208	4	5.1	07229−1115
*J*07493726−3820439	CMa		183.7	68.4	9.183	2.448	0.230	8	2.5	07478−3813
*J*08003235−3559477	CMa		190.0	66.3	8.045	1.508	0.851	9	1.6	07586−3551
*J*08144298−3233047	CMa	−139.1	197.1	63.0	8.439	2.173	0.203	7	9.4	08127−3223
*J*08160288−3536539	CMa		197.8	66.0	9.296	1.969	2.185	10	1.6	08141−3527
*J*08333853−3707051	CMa		207.0	67.3	7.026	1.318	0.263	6	1.7	08317−3656
*J*08451851+1420341	Sgr		204.8	15.8	12.379	0.969	0.009	> 30		
*J*09322353+1146033	Sgr		217.0	16.9	9.589	1.184	0.008	21	2.0	09296+1159
*J*11392617+2743564	Sgr		241.1	−6.9	13.036	2.047	0.009	> 30		
*J*13122380+0051472	Sgr		273.1	7.0	12.650	2.360	0.013	> 30		
*J*13330290−2317496	Sgr		290.7	25.1	13.442	1.100	0.037	> 30		
*J*14572697+0516034	Sgr		293.7	−10.0	11.438	1.238	0.015	> 30		C star*
*J*16075796−2040087	Sgr		321.4	4.6	7.808	1.497	0.128	8	1.5	16050−2032
*J*16465797+7931489	Sgr		216.7	−64.8	13.927	1.276	0.016	> 30		
*J*19235554−1302029	Sgr	66.9	4.2	−16.7	9.747	1.467	0.065	19	1.1	19211−1307
*J*23164760−2723338	Sgr		56.6	4.7	11.462	2.475	0.010	22		

§ P-M relation, $M_K = 6.43$ at 8 kpc for P=450 days, was used.

* from Mauron et al. (2005).

Table 5. The values of the best parameters of the warp from SiO maser data.

Sample	Data points	b_0 (deg)	ϕ_0 (deg)	R
Disk only ($\|b\| < 3^\circ$)	79	0.50 ($\pm$1.16)	25.6 ($\pm$17.5)	0.049
Whole ($\|b\| < 5^\circ$)	108	3.09 ($\pm$1.62)	28.4 ($\pm$4.0)	0.182
Velocity limited ($\|b\| < 5^\circ$ with $V_{lsr} > 50$ km s^{-1})	48	2.23 ($\pm$2.27)	19.8 ($\pm$10.1)	0.141

Table 6. Properties of maser sources with $V_{\rm LSR} < -50$ km s^{-1}.

IRAS name	Other name	l (deg)	b (deg)	$V_{\rm LSR}$ km s^{-1}	K (mag)	$H-K$ (mag)	K_c (mag)	F_{12} (Jy)	C_{12}
18307+0102	OH031.8+04.5	31.817	4.537	$-62.8^\dagger$	6.902	1.561	5.374	6.4	0.111
18325−0721	OH024.581+00.224	24.581	0.224	-72.6^*	—$^\flat$	—	—	5.3	0.340
18387−0951		23.078	−2.274	$-62.8^\ddagger$	12.215	1.075	11.387	7.0	0.299
18393−1020	OH022.707−02.631	22.707	−2.631	-76.1^*	6.934	1.400	5.638	5.9	−0.070
18399−0149	OH030.336+01.171	30.336	1.171	-64.7^*	4.607	0.899	4.032	12.1	−0.134
18465−0717	OH026.246−02.814	26.246	−2.814	-65.8^*	7.886	2.876	4.465	$16.4^\S$	$0.010^\S$
19195−1423		23.448	−13.220	$-75.3^{\ddagger\P}$	5.598	1.400	4.302	8.8	0.170
19263−1922		19.466	−16.779	$-68.8^\P$	4.220	0.570	4.119	11.9	−0.190
19281−1646		22.122	−16.110	$-75.2^{\ddagger\P}$	5.054	1.086	4.210	24.7	−0.110

* Sevenster et al. 2001
† Eder et al. 1988
‡ te Lintel-Hekkert et al. 1991
¶ Present work.
$^\flat$ not identified in 2MASS database, but seen on the Spitzer GLIMPSE image; see Deguchi et al. 2007.
§ Apparent double sources; flux densities not reliable (Deguchi et al. 1999).

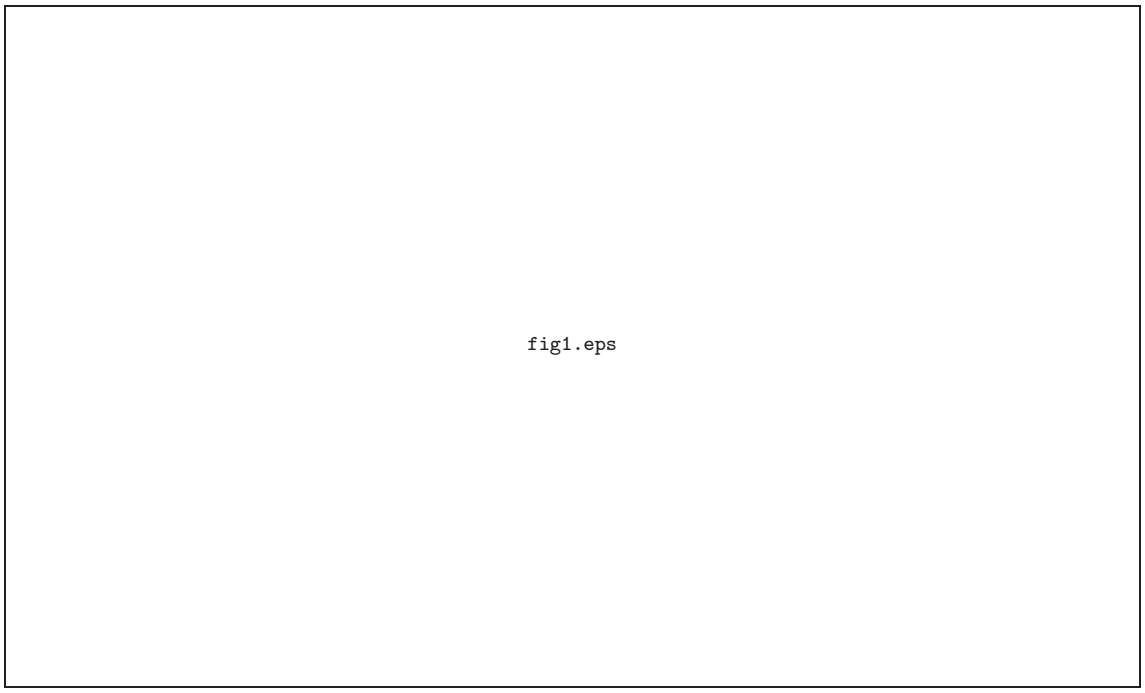

Fig. 1. Distribution of the observed sources in the Galactic coordinates in the Hammer-Aitoff's projection. The dotted curve indicates the orbital plane of SagDEG.

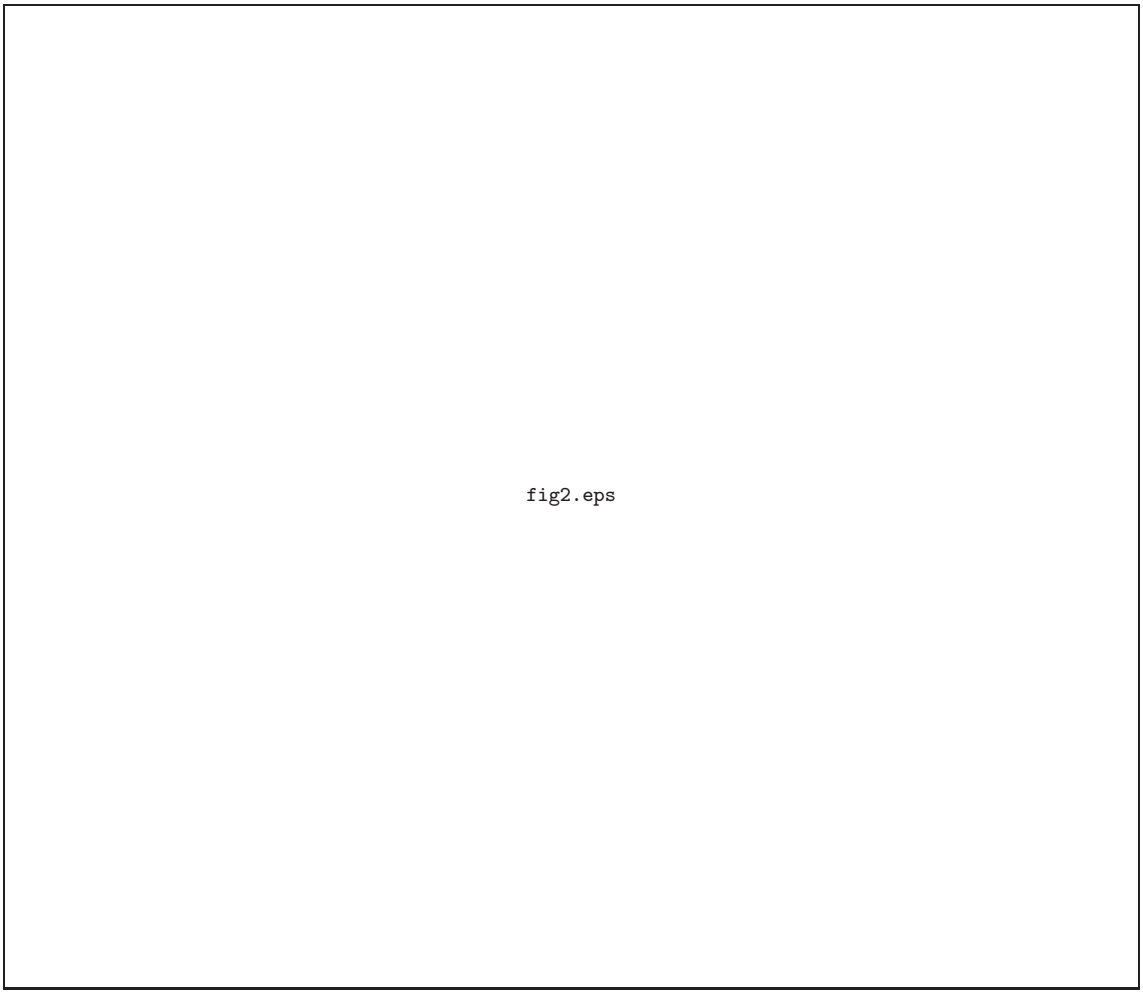

Fig. 2. Plots of K versus $H-K$ and F_C versus C_{CE}. Filled and unfilled circles indicate SiO detection and nondetection.

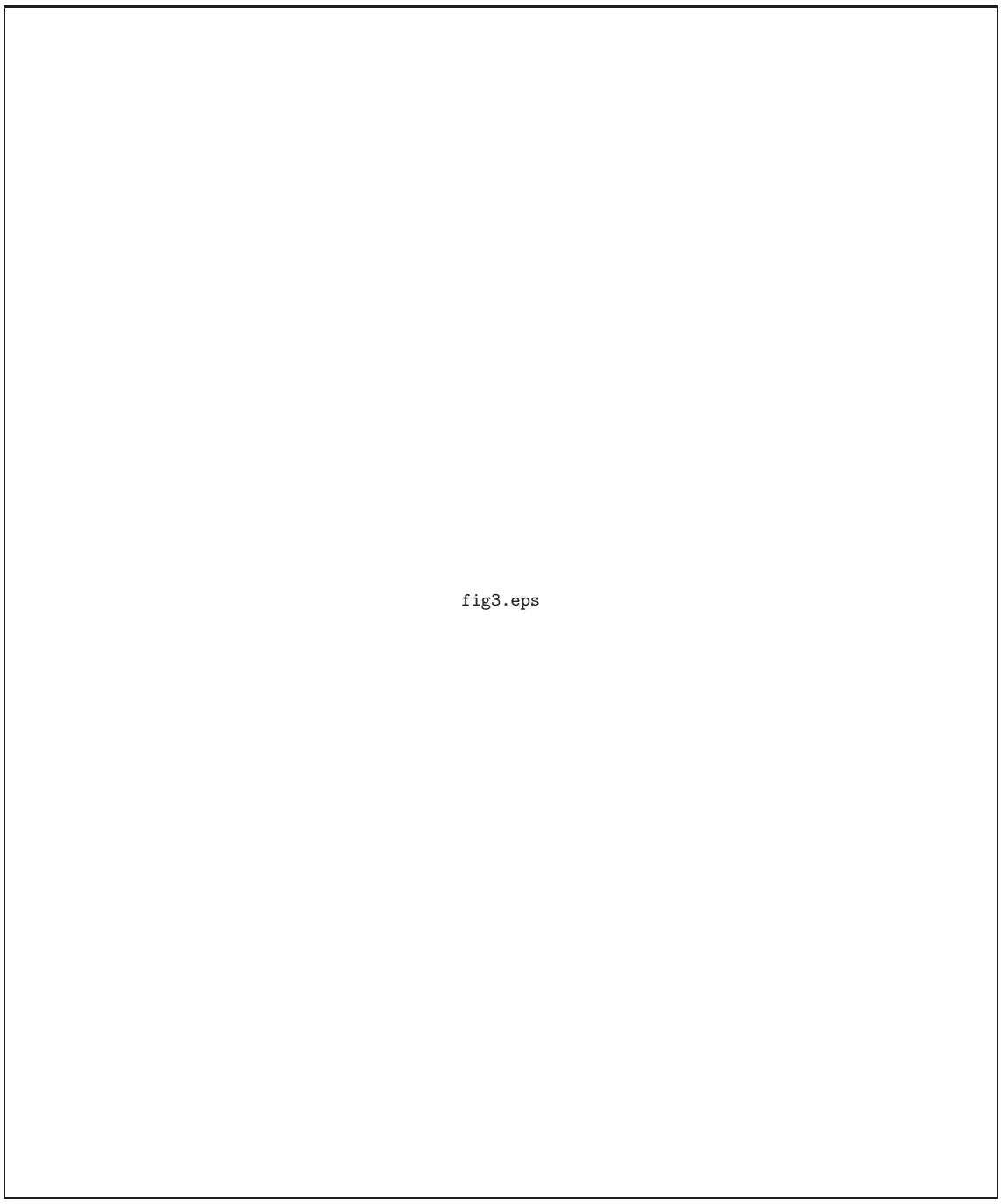

Fig. 3. Velocity distribution of the observed sources in the ranges $-40^\circ < l < 50^\circ$ (top) and $180^\circ < l < 270^\circ$ (bottom). The solid and broken curves indicate the velocities expected from the Galactic rotation curve, which is assumed to be flat at 220 km s^{-1} or linear within 1 kpc from the Galactic center. One object with $V_{\rm lsr} = -261.5$ km s^{-1} ($J17335931-2659216$), is out of this figure. The star J05475868 is a candidate for the dwarf galaxy association, and the stars J06353168 and J08144298 are likely disk objects (see section 3.1 and appendix).

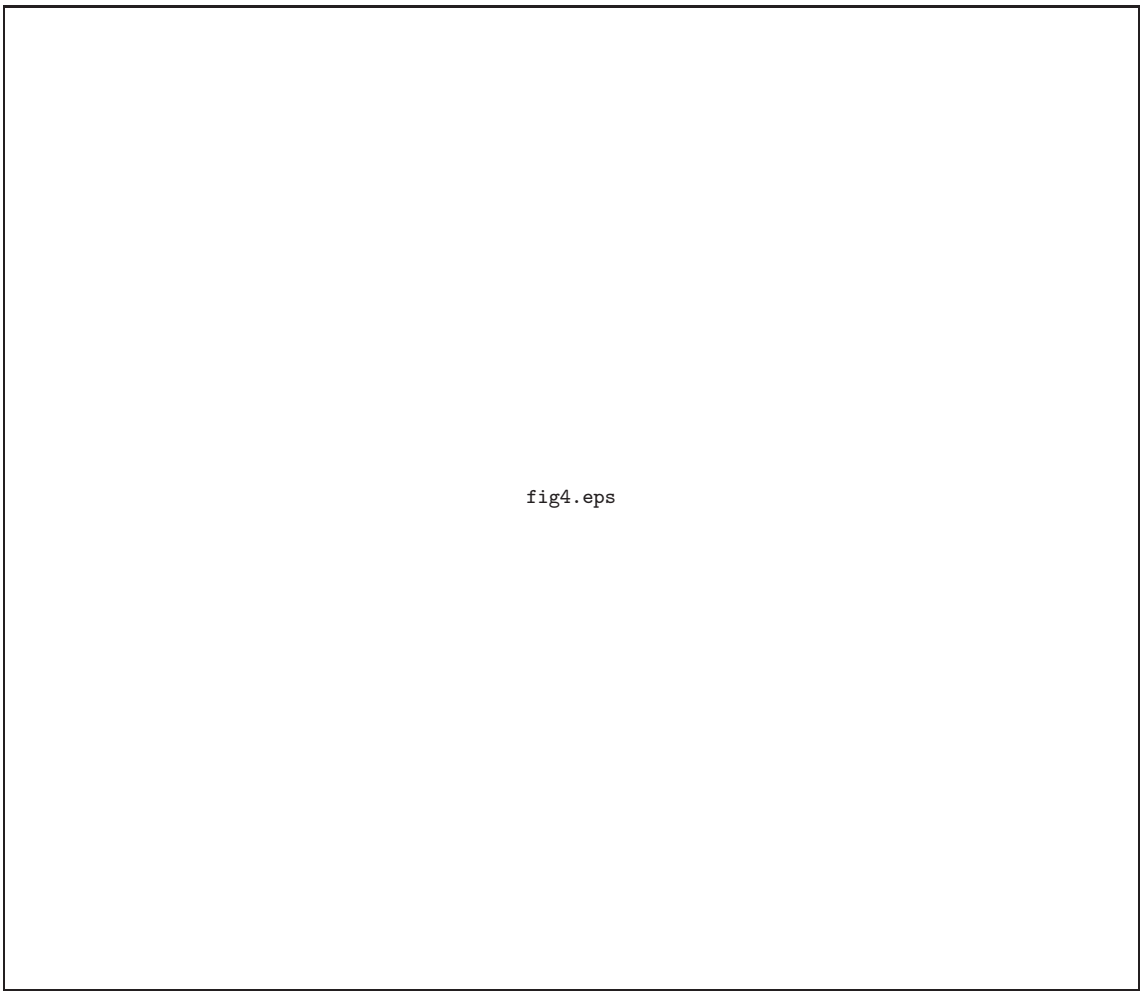

Fig. 4. Velocity distribution of the SiO maser sources in the Sgr coordinates. Blue diamonds indicate the SiO maser sources detected in this paper, and the large filled red circle indicates the candidate for SagDEG tidal-tail associations, $J1923554-1302029$. Black squares indicate the M giants sampled by Majewski et al. (2004) and the thin broad bands are result of simulation of the tidal tail of SagDEG, which were taken from Law et al. (2005).

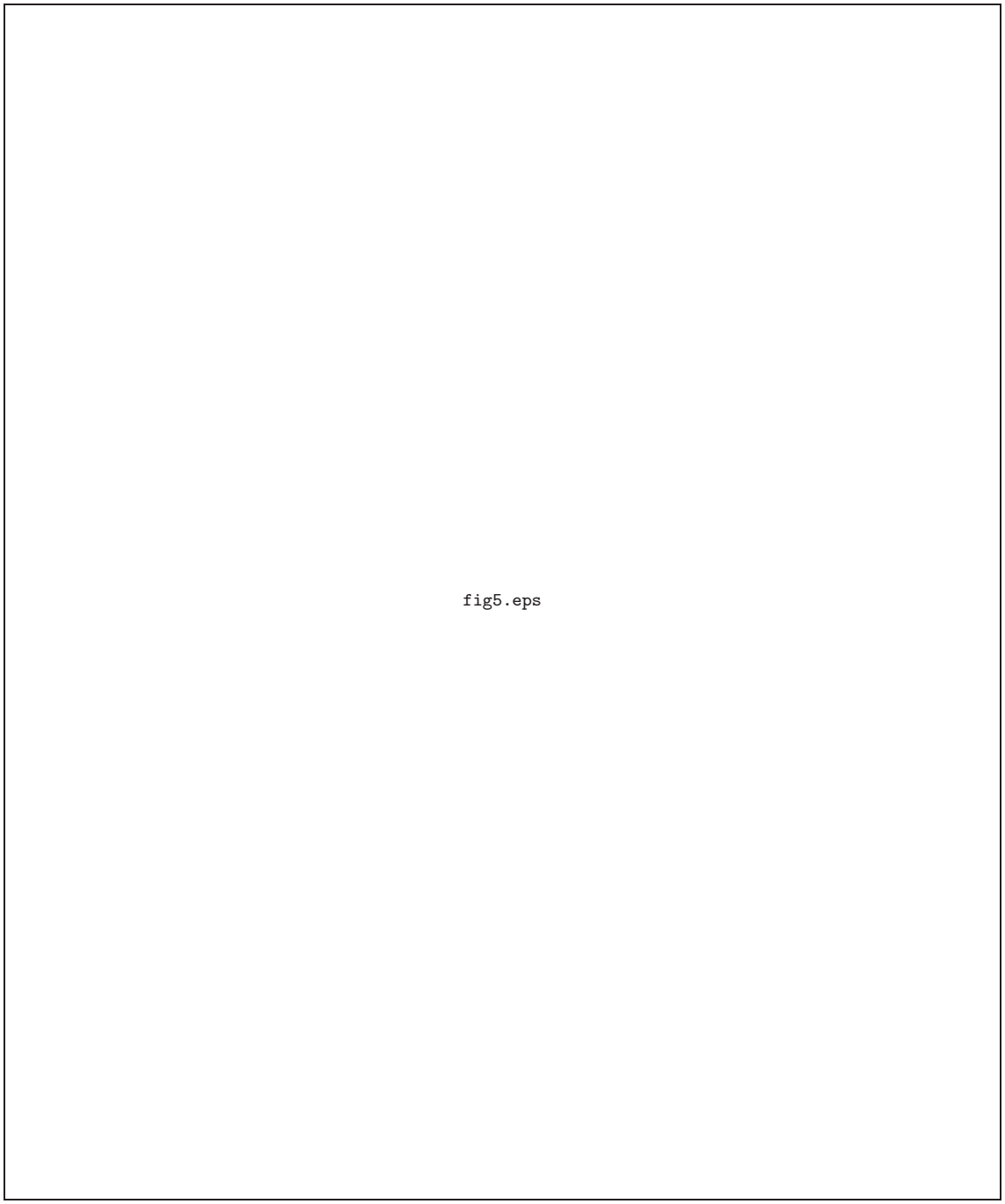

Fig. 5. Comparison of velocity distributions for objects above and below $|b| = 3^\circ$ (top), and another comparison for upper disk objects with $b > 3^\circ$ and $b < -3^\circ$ (bottom). All the objects plotted have $|b| < 6^\circ$. The cross in the top panel indicates the position of the most significant difference in fraction between two samples from a 2-d Kolmogorov-Smirnov test.

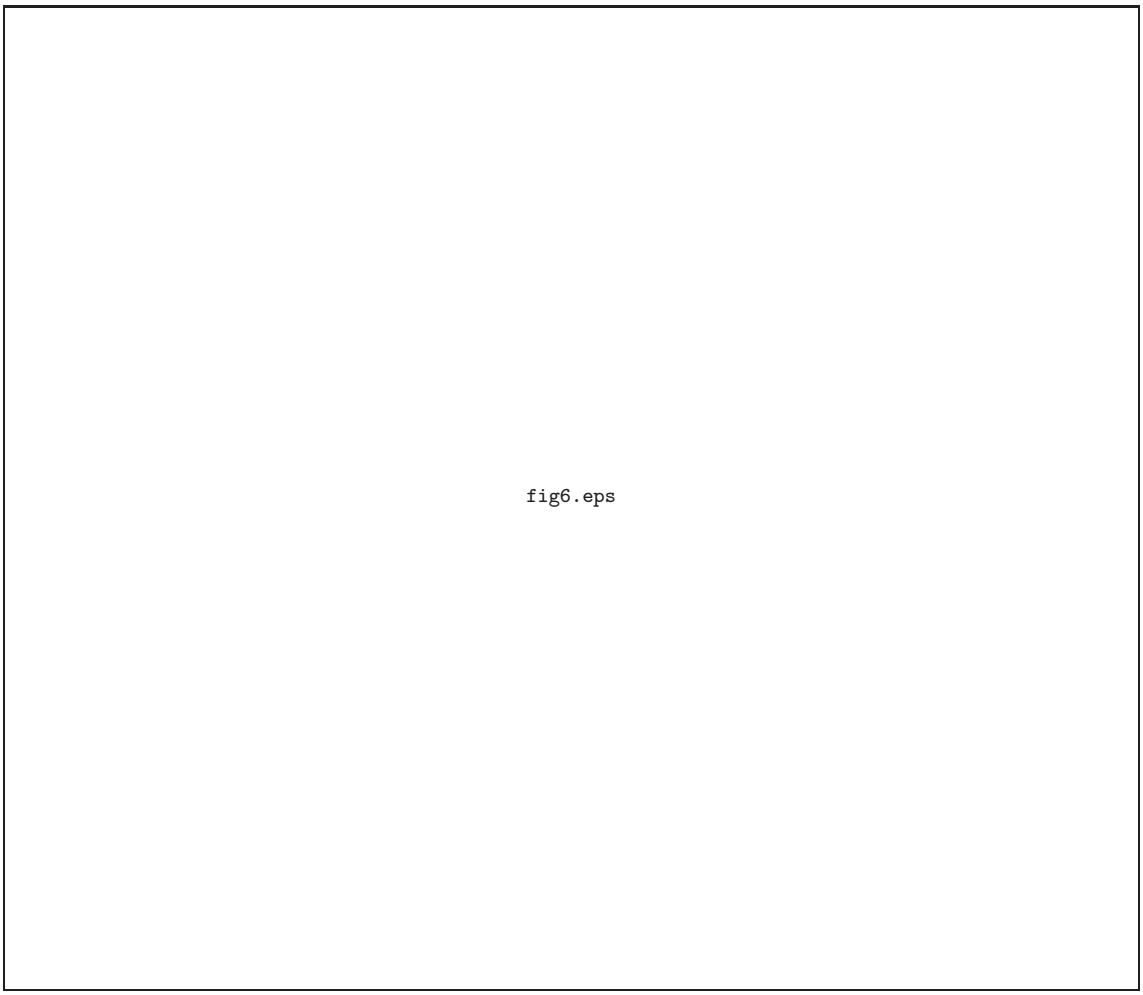

Fig. 6. Source distribution in Galactic coordinates. The small and large open circles indicate the disk sample ($|b| < 3^\circ$) and whole sample ($|b| < 5^\circ$). Filled circles indicates a subsample of distant objects ($V_{lsr} > 50$ km s^{-1}). There is a concentration of 4 sources within 1 degree at (26.3°, 3.3°), but this seems a chance coincidence, because their radial velocities are very diverse from −15 to 86 km s^{-1}. The thin ellipse at the lower right part indicates a concentration of relatively nearby stars asymmetric with respect to the Galactic plane. The best-fit linear line for each sample [minimizing square sum of residue $y_i = b_i - b_0 \times sin(l_i - \phi_0), \quad (i = 1, ..., n)$] is shown.

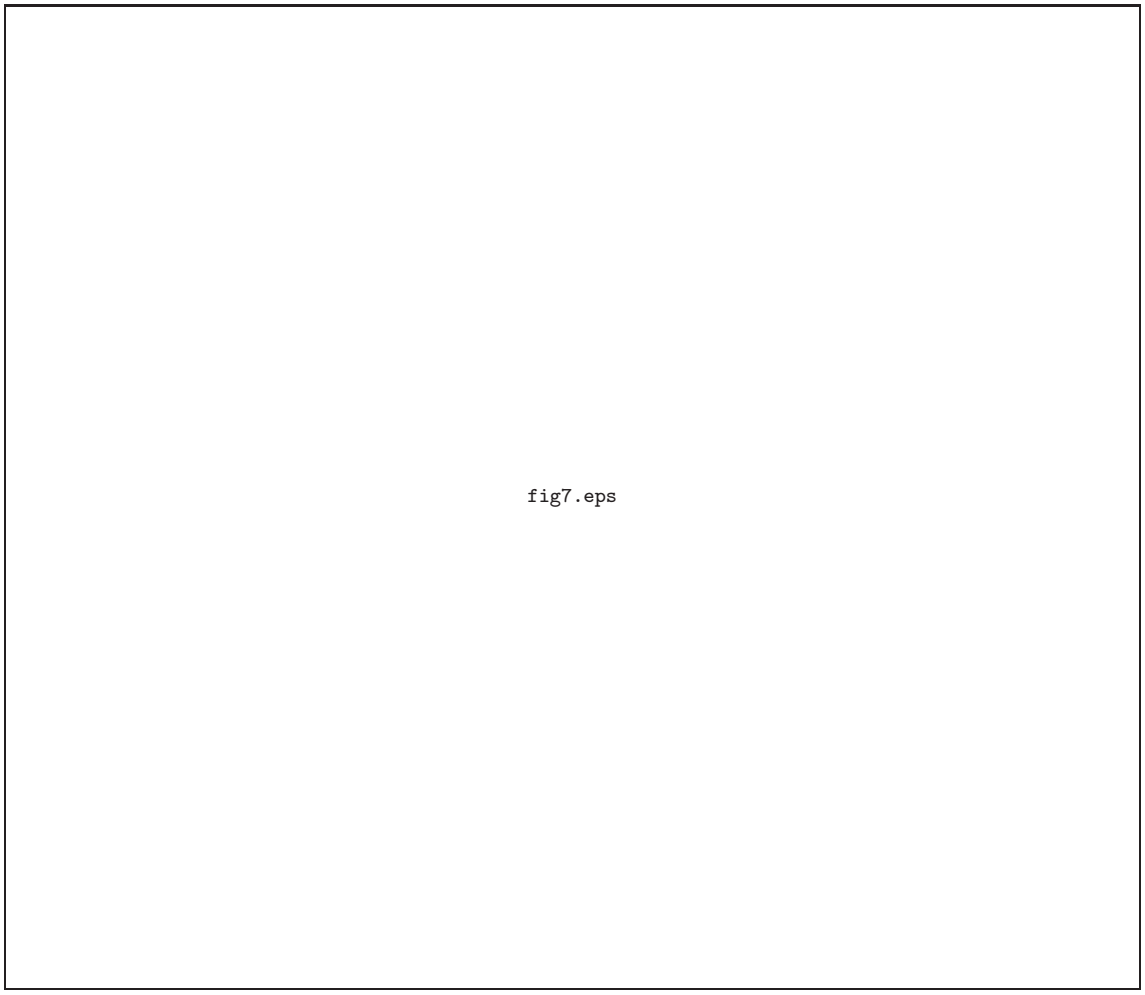

Fig. 7. Distribution of SiO/OH maser sources with $V_{\rm LSR} < -50$ km s^{-1} (filled circles). Positions of the nearby Globular clusters are indicated by open squares; data are taken from Harris (1996) except GLIMPSE C01 (Kobulnicky et al. 2005). The broken line indicates the least squares fit to the Galactic coordinates of maser sources; $l = 0.39\ (\pm 0.11) \times b + 27.0^\circ\ (\pm 1.1^\circ)$, where the values between parentheses are standard errors of the coefficients.

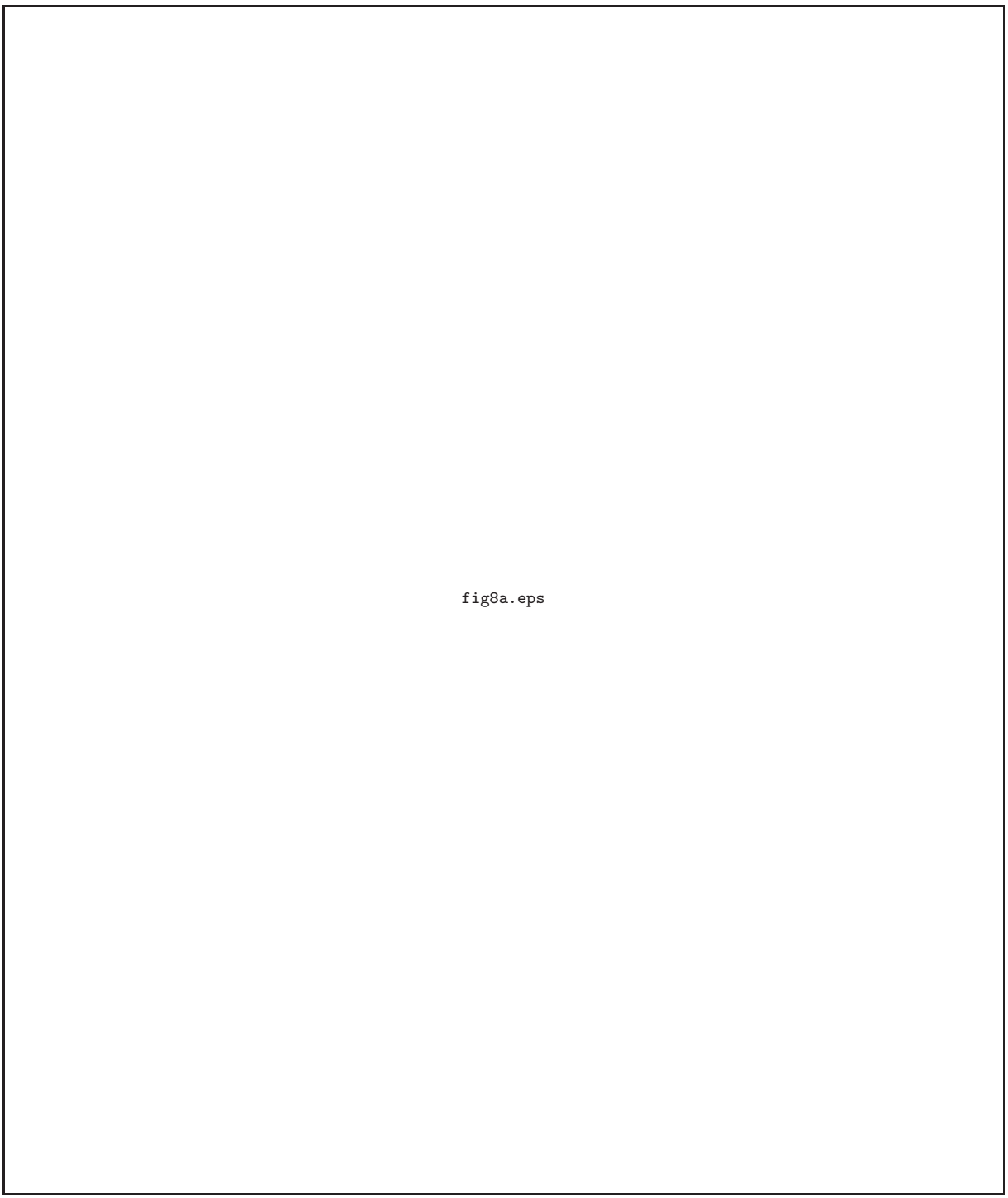

Fig. 8. a. Spectra of new SiO detections. The previous detections are not shown. The 2MASS name (first half) and observed date (yymmdd.d) are shown on the upper left in each panel.

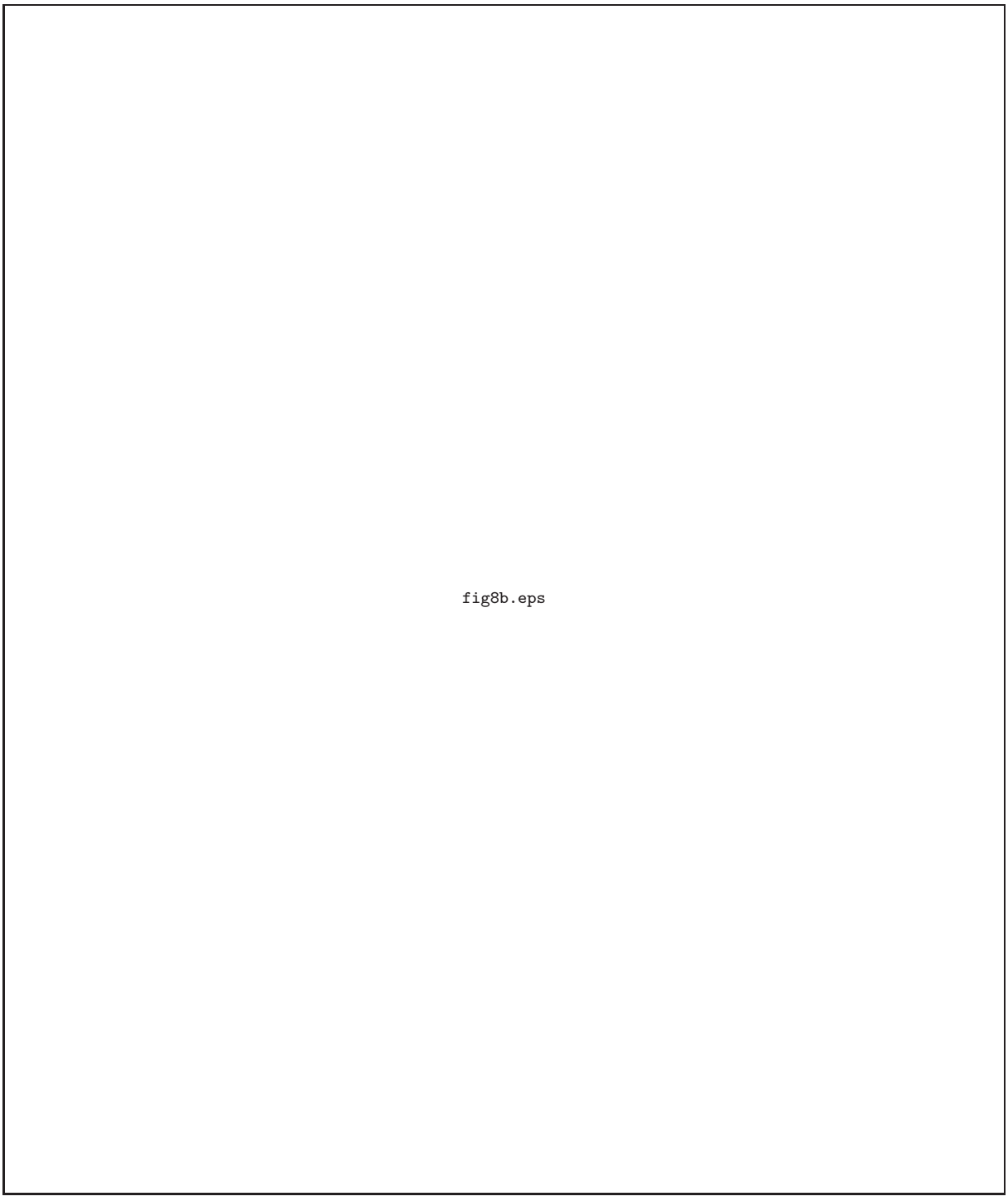

Fig. 8. b. continued

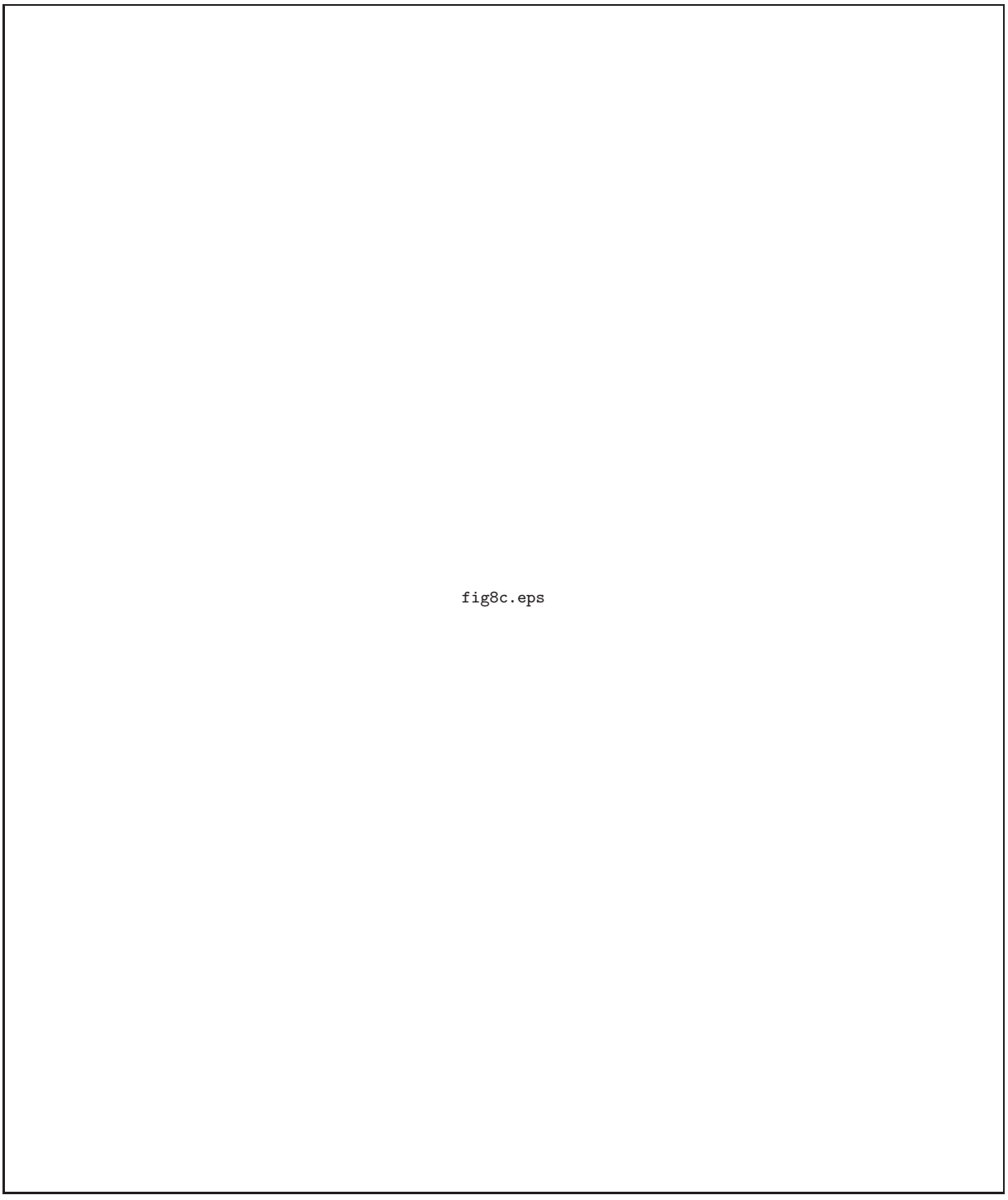

Fig. 8. c. continued

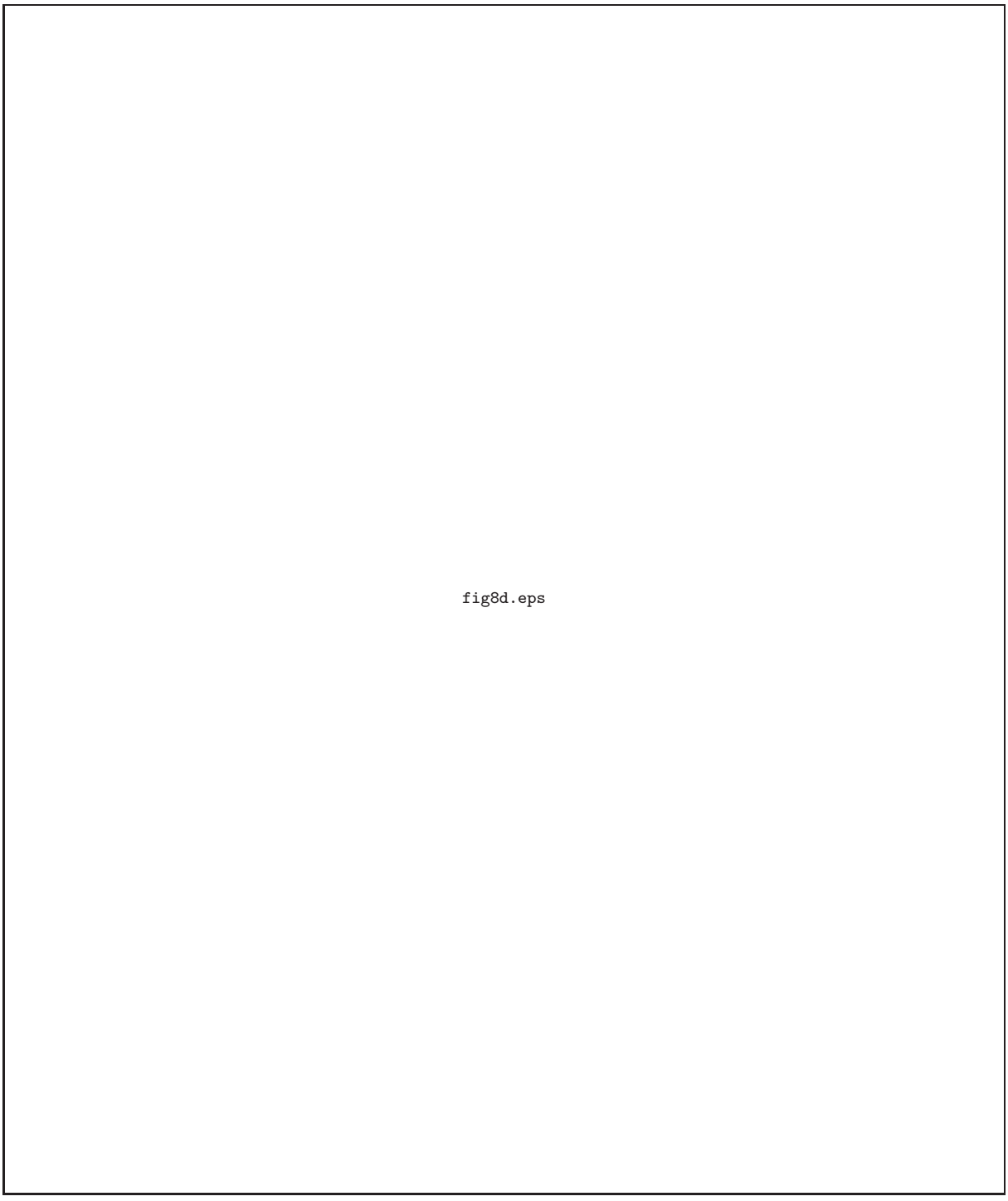

Fig. 8. d. continued

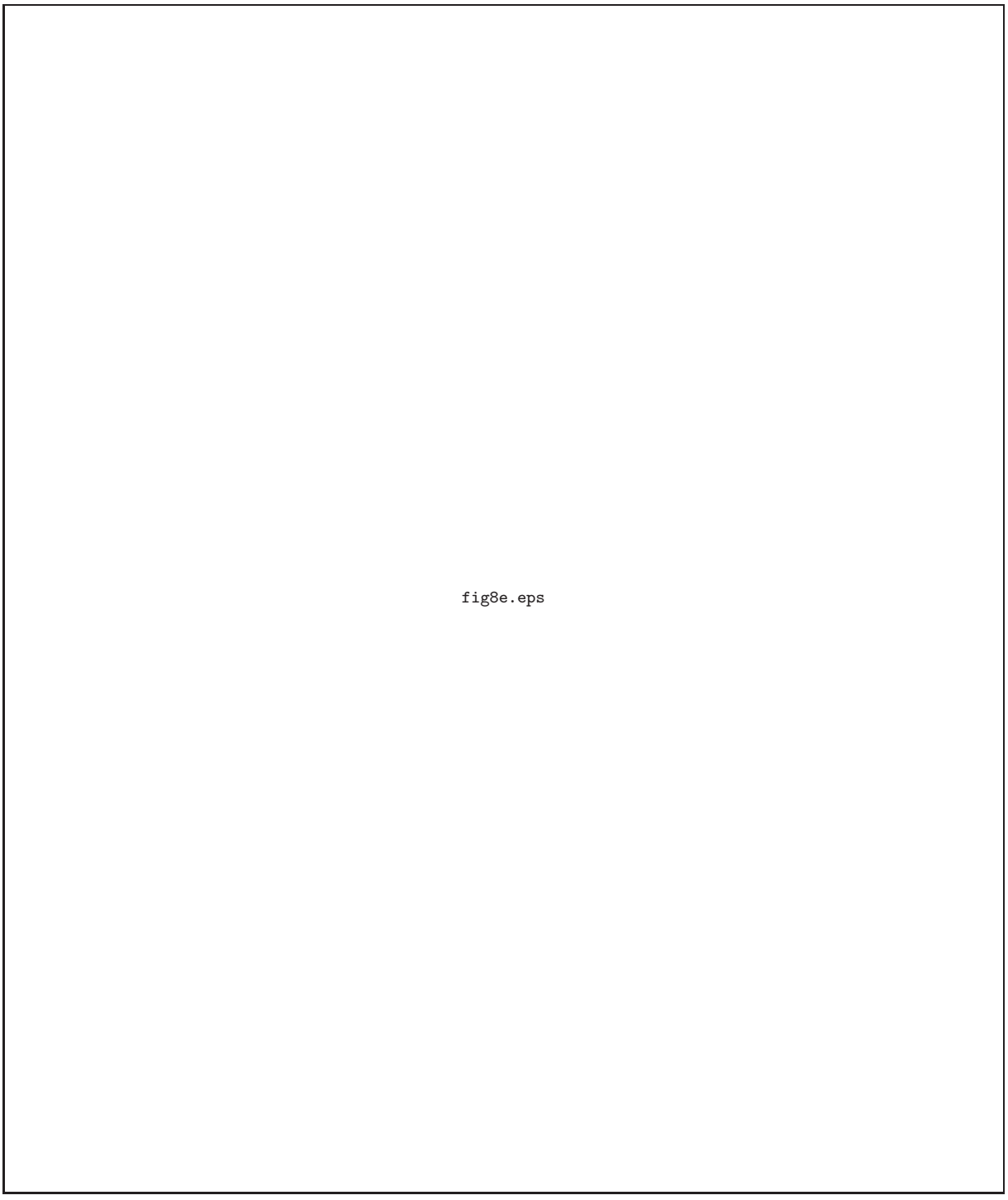

Fig. 8. e. continued

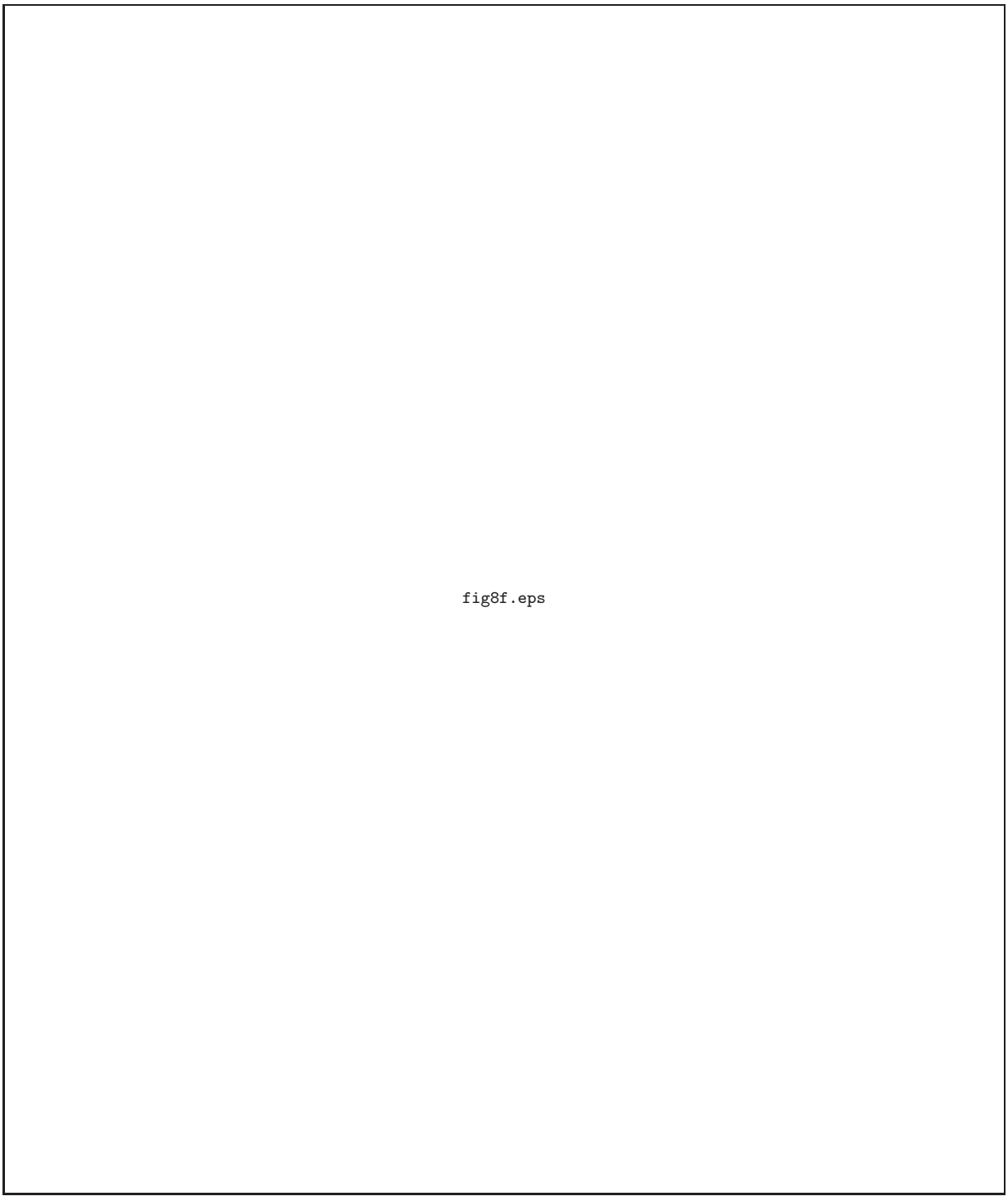

Fig. 8. f. continued

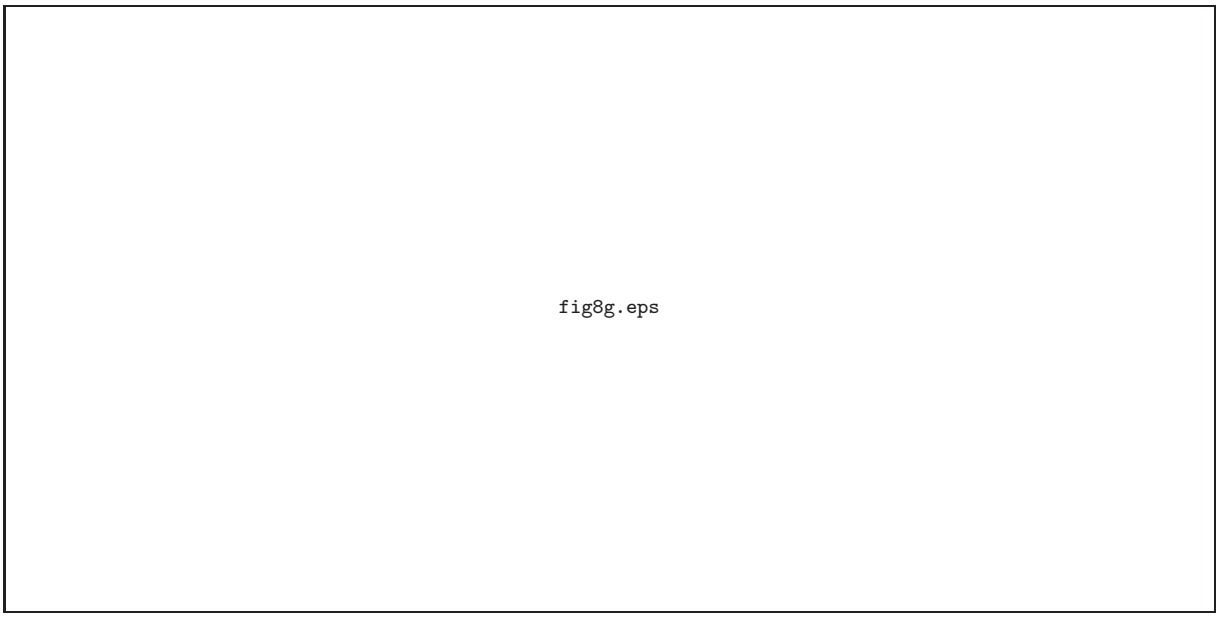

Fig. 8. g. continued

This figure "fig1.jpg" is available in "jpg" format from:

http://arXiv.org/ps/0704.1713v1

This figure "fig2.jpg" is available in "jpg" format from:

http://arXiv.org/ps/0704.1713v1

This figure "fig3.jpg" is available in "jpg" format from:

http://arXiv.org/ps/0704.1713v1

This figure "fig4.jpg" is available in "jpg" format from:

http://arXiv.org/ps/0704.1713v1

This figure "fig5.jpg" is available in "jpg" format from:

http://arXiv.org/ps/0704.1713v1

This figure "fig6.jpg" is available in "jpg" format from:

http://arXiv.org/ps/0704.1713v1

This figure "fig7.jpg" is available in "jpg" format from:

http://arXiv.org/ps/0704.1713v1

This figure "fig8a.jpg" is available in "jpg" format from:

http://arXiv.org/ps/0704.1713v1

This figure "fig8b.jpg" is available in "jpg" format from:

http://arXiv.org/ps/0704.1713v1

This figure "fig8c.jpg" is available in "jpg" format from:

http://arXiv.org/ps/0704.1713v1

This figure "fig8d.jpg" is available in "jpg" format from:

http://arXiv.org/ps/0704.1713v1

This figure "fig8e.jpg" is available in "jpg" format from:

http://arXiv.org/ps/0704.1713v1

This figure "fig8f.jpg" is available in "jpg" format from:

http://arXiv.org/ps/0704.1713v1

This figure "fig8g.jpg" is available in "jpg" format from:

http://arXiv.org/ps/0704.1713v1